How natural processes contribute to flood protection

A sustainable adaptation scheme for a wide green dike

Marijnissen, Richard; Esselink, Peter; Kok, Matthijs; Kroeze, Carolien; van Loon-Steensma, Jantsje

DOI
10.1016/j.scitotenv.2020.139698

Publication date
2020

Document Version
Final published version

Published in
Science of the Total Environment

Citation (APA)
Marijnissen, R., Esselink, P., Kok, M., Kroeze, C., & van Loon-Steensma, J. (2020). How natural processes contribute to flood protection: A sustainable adaptation scheme for a wide green dike. *Science of the Total Environment*, *739*, 1-17. Article 139698. https://doi.org/10.1016/j.scitotenv.2020.139698

Science of the Total Environment 739 (2020) 139698

Contents lists available at ScienceDirect

Science of the Total Environment

journal homepage: www.elsevier.com/locate/scitotenv

How natural processes contribute to flood protection - A sustainable adaptation scheme for a wide green dike

Richard Marijnissen [a,*], Peter Esselink [b], Matthijs Kok [c,d], Carolien Kroeze [a], Jantsje M. van Loon-Steensma [a,c]

[a] Water Systems and Global Change group, Wageningen University & Research, P.O. Box 47, 6700 AA Wageningen, the Netherlands
[b] PUCCIMAR, Ecological Research and Consultancy, Boermarke 35, 9481 HD Vries, the Netherlands
[c] Faculty of Civil Engineering and Geosciences, Delft University of Technology, P.O. Box 5048, 2600 GA Delft, the Netherlands
[d] HKV Consultants, Botter 11 29, 8232 JN Lelystad, the Netherlands

HIGHLIGHTS

- 9.4 ha of pit can reinforce a 1 km dike section until 2100 under sea-level rise.
- The infill rate of the borrow pit increases with its depth.
- Infilling of the borrow pit is projected to accelerate with sea-level rise.

GRAPHICAL ABSTRACT

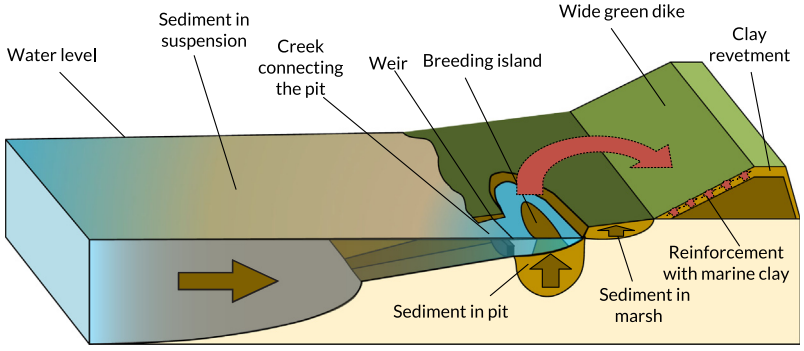

ARTICLE INFO

Article history:
Received 1 November 2019
Received in revised form 9 April 2020
Accepted 23 May 2020
Available online 02 June 2020

Editor: Jan Vymazal

Keywords:
Nature-based solutions
Climate adaptation
Salt marsh
Sea-level rise
Clay mining
Flood risk

ABSTRACT

Effective adaptation to sea-level rise is critical for future flood protection. Nature-based solutions including salt marshes have been proposed to naturally enhance coastal infrastructure. A gently sloping grass-covered dike (i.e. Wide Green Dike) can be strengthened with clay accumulating locally in the salt marsh. This study explores the feasibility of extracting salt-marsh sediment for dike reinforcement as a climate adaptation strategy in several sea-level rise scenarios, using the Wide Green Dike in the Dutch part of the Ems-Dollard estuary as a case study. A 0-D sedimentation model was combined with a wave propagation model, and probabilistic models for wave impact and wave overtopping. This model system was used to determine the area of borrow pits required to supply clay for adequate dikes under different sea-level rise scenarios.

For medium to high sea-level rise scenarios (>102 cm by 2100) thickening of the clay layer on the dike is required to compensate for the larger waves resulting from insufficient marsh accretion. The model results indicate that for our case study roughly 9.4 ha of borrow pit is sufficient to supply clay for 1 km of dike reinforcement until 2100. The simulated borrow pits are refilled within 22 simulation years on average, and infilling is projected to accelerate with sea-level rise and pit depth. This study highlights the potential of salt marshes as an asset for adapting flood defences in the future.

1. Introduction

Coastlines are expected to become increasingly vulnerable to flooding from a combination of rising sea-levels due to climate change

* Corresponding author.
E-mail address: richard.marijnissen@wur.nl (R. Marijnissen).

https://doi.org/10.1016/j.scitotenv.2020.139698

and economic growth (Neumann et al., 2015; Nicholls, 2004). Accelerated sea-level rise from future ice-loss in the Antarctic, among other factors, considerably raises the sea-level projection for the end of the 21st century (DeConto and Pollard, 2016). The large range in future sea-level rise predictions has prompted the search for robust yet flexible adaptation options for the world's vulnerable delta regions (Hallegatte, 2009). Many studies (Borsje et al., 2011; Möller et al., 2014; Temmerman et al., 2013; van Loon-Steensma, 2015; van Loon-Steensma et al., 2016; Vuik et al., 2018) stress the capacity and importance of specific coastal ecosystems such as salt marshes and mangroves to dampen wave action and preserving foreshores. Incorporating these systems into coastal management could reduce the need for more costly flood protection measures in the future. As a result, nature-based flood-protection measures have emerged as a potential adaptation option.

The tendency of coastal wetlands to accumulate sediment provides an avenue for incorporating them in flood protection strategies. In natural salt marshes, the vegetation decelerates tidal currents by exerting friction which allows suspended sediment to accumulate on the marsh platform (Bouma et al., 2005; Christiansen et al., 2000; Leonard and Croft, 2006). Furthermore, roots bind the marsh bed and reduce erosion during storm conditions. Provided there is a sufficient supply of sediment, a marsh accumulates fine sediment based on the sea-level, the tide, compaction and subsidence processes, organic deposition, and wave action (Allen, 2000b; Davidson-Arnott et al., 2002).

The rising of the marsh platform by sediment accumulating within the marsh has the benefit of reducing the load on flood protection infrastructure (Vuik et al., 2019). Another benefit of sedimentation of salt marshes for flood protection is to supply clay as building material for dike reinforcement, as was done historically. Within the German sector of the Wadden Sea, pits have already been excavated for dike reconstruction and to rejuvenate marsh from a late stage of succession. At Petersgroden in 1998 approximately 150,000 m^3 of clay was extracted from a 300 × 330 m (10 ha) pit with a depth of 1.2 to 1.5 m. Initially the infilling rate was 15 cm/yr in the first years and decelerated to 4 cm/yr by 2007 (Bartholomä et al., 2013). More recently in 2012 at Elisabethaußengroden 325,000 m^3 of clay was excavated across four pits to cover roughly 1/3 of the clay demand for reinforcing a 27-km long dike section (Menke, 2015). Infilling of the pit, and accretion of marshes in general, relies on inundation by sediment-laden water from the sea. As the bottom elevation of the pit increases, it becomes increasingly reliant on spring- and storm tides to supply additional sediment and the thus the infilling rate decelerates (Bartholomä et al., 2013). From experience pits are refilled within 30 years after excavation (Arens, 2002; Bartholomä et al., 2013).

While sedimentation within marshes can be an asset in flood protection it is yet unclear how future sea-level rise can affect such a strategy in the long term. Both the historic and foreseen response of marshes to sea-level rise has been extensively studied. Many marshes are expected to drown within this century as these will not be able to accrete fast enough to keep pace with sea-level rise (Best et al., 2018; Crosby et al., 2016; Kirwan et al., 2010; Schuerch et al., 2018). The response of borrowing pits within them has, however, not been studied so far. Therefore, the effectiveness of incorporating borrowing pits for dike-building material as a measure for sea-level rise adaptation is still unknown.

This study explores the feasibility of extracting sediment for dike reinforcements from the fringing salt marshes as a climate adaptation strategy in several sea-level rise scenarios, using the Wide Green Dike in the Dutch sector of the Dollard bay in the Ems estuary as a case study. To sustain adaptation of the flood defence by natural sedimentation of the marsh under sea-level rise, two conditions need to be satisfied: the borrow pit will refill to the marsh's level and the dike meets the national flood protection standard. This study explores 1) the feasibility and 2) sustainability of extracting salt marsh sediment for dike reinforcements as a climate adaptation strategy in several sea-level rise scenarios. A 0-D sedimentation model was combined with a wave propagation model, and probabilistic models for wave impact and wave overtopping. This model system was used to determine the dimensions of adequate dikes and borrow pit dimensions under different sea-level rise scenarios.

2. The study area

2.1. History of the Dollard

The Dollard forms a bay of about 100 km^2 within the Ems estuary located on the Dutch-German border in the Wadden Sea (Fig. 1). Around 80% of the Dollard consists of tidal flats on which approximately 1.1 km^2 of salt marsh is present. The Dollard has a mesotidal regime with a tidal range of 3.3 m and a mean high tide of 1.55 m + NAP (Dutch Ordnance Level).

The bay developed during the Middle Ages and reached its greatest extent in the 16th century after a series of storm surges (Esselink, 2000). Further transgressions were halted by improved management of the dikes. Land was reclaimed from the sea by repeatedly embanking the emerging marshes on the fringes of the diked estuary. The last reclamation was completed in 1924 (Esselink, 2000). In the Dollard, engineering measures to promote salt-marsh development were initiated as early as the 17th century. This was achieved by the construction and upkeep of a pattern of low clay-built groynes and a dense drainage network (Esselink, 1998). These works were acquired and expanded by the Provincial Government in 1938 but were discontinued 15 years later. The majority of the present-day salt marshes date back to this period (1938–1953) (Esselink, 1998). The historic loss of intertidal area for the deposition of sediment, among others through deepening of the estuary for navigation and ongoing morphological processes, has been linked to an increasingly high turbidity in the estuary today (van Maren et al., 2016) which inhibits the primary production of the local marine ecosystem (DeGroodt and de Jonge, 1990).

2.2. The Wide Green Dike pilot

Dikes along the Dutch Dollard coast were designed for an acceptable anual failure probability of 1/3000. In the last dike assessment only 20% of the Dollard dikes met the safety standard (van Loon-Steensma and Schelfhout, 2017). The current dikes feature a crest height between 7.7 and 9.3 m + NAP a lower section of the seaward slope at an angle of 1:4 and an upper section at an angle of 1:7. The lower section of the slope is reinforced with asphalt and stones against wave impacts while the remaining upper section consists of grass (van Loon-Steensma and Schelfhout, 2017).

The Province of Groningen aims to remove 1 million ton of sediment from the estuary annually to reduce the high turbidity in the estuary to acceptable levels (Provincie Groningen and Ministerie van Infrastructuur en Milieu, 2018). A so-called “Wide Green Dike” has emerged as an option to reinforce the dikes while reducing turbidity within the estuary. As a pilot 1 km of dike will be reinforced with marine clay extracted locally from the salt marsh (Hunze en Aa's, 2020). The resulting borrow pit will function as a sink for new sediment while the excavated clay is processed for dike reinforcement. The dike will feature a shallow (1:7) grass outer slope along the entire seaward side to withstand the impact of large waves rather than a conventional stone or asphalt revetment. Furthermore, it simplifies future reinforcements with the excavated clay (van Loon-Steensma and Schelfhout, 2013; van Loon-Steensma and Schelfhout, 2017).

The borrow pit will extract sediment from the water by a similar process as the marsh. Water carrying sediment in suspension is transported landward during flood tide. Within the marsh and pit the flow of water is decelerated allowing the suspended sediment to settle. Because of its depth the pit will experience more regular inundations of sediment-laden water than the marsh through a creek leading into it,

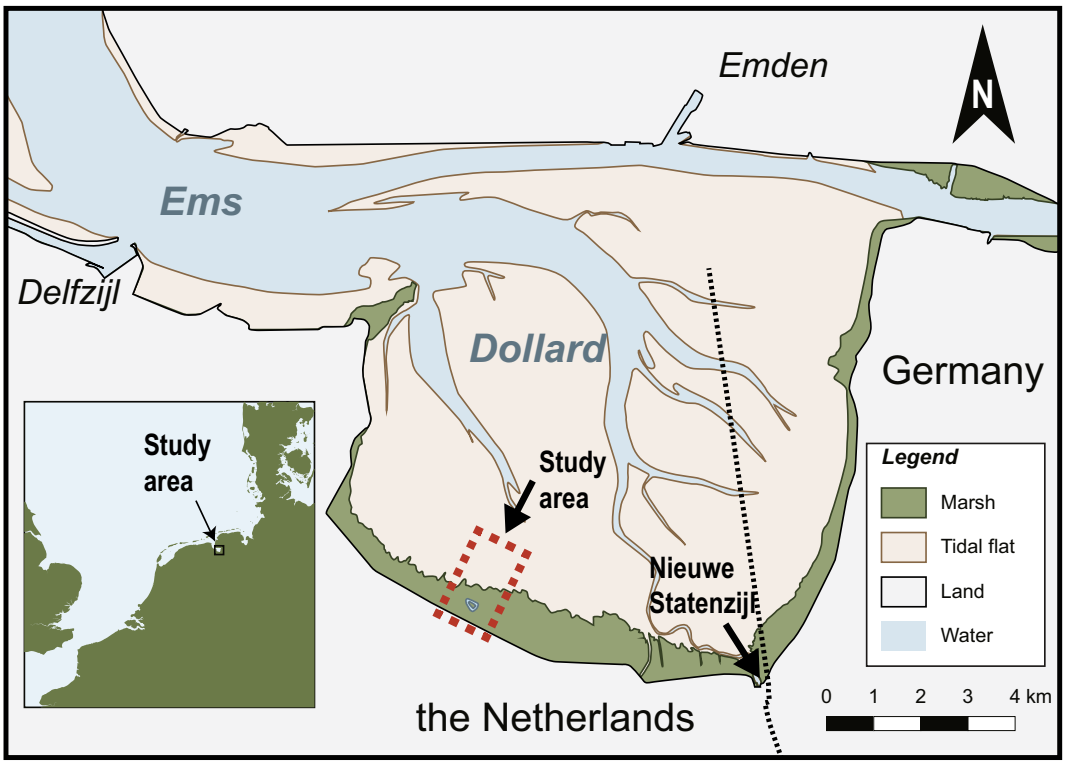

Fig. 1. Location of the study area where the pilot study for clay mining is being conducted within the Ems-Dollard estuary.

thereby capturing more suspended sediment from the estuary over time until the pit is filled.

At the time of writing a pilot project of the Wide Green Dike is being conducted in the Dollard (see Fig. 2) (Hunze en Aa's, 2020). In the spring of 2018 45,000 m^3 of clay was excavated from a 4 ha borrow pit with an average depth of 1.6 m (Esselink et al., 2019). The pit is connected to the tidal creek through a weir (of 0.9 m + NAP) which impedes the in- and outflow. At the centre of the pit an elevated section of marsh remains to serve as a breeding island for birds. The excavated clay is being processed to be used as dike clay. Meanwhile the infilling of the borrow pit and ecological impacts are being monitored.

3. Methods

3.1. Modelling approach

To assess the feasibility of a wide green dike system under sea-level rise, both the clay required for dike reinforcement and the future clay yield from the pit need to be predicted. We do this in three modelling steps in which we quantify: 1) on the foreshore the accretion of both the marsh and the pit over time, 2) the change in storm conditions over time, 3) the failure probability of a dike design subjected to those storm conditions (see Fig. 3) as assessed with the official Dutch dike assessment tools. The final step is repeated for different dike designs to find the design that requires the lowest amount of clay.

In the first step the vertical marsh growth and infilling of the borrow pit in response to different sea-level rise scenarios is modelled by a 0D numerical deposition model which has been used in many other studies (Allen, 1990; French, 1993; Krone, 1987; Temmerman et al., 2003). The simplicity and speed of the 0D model allows for uncertainties to be quantified by varying the initial elevation and sediment properties in a Monte Carlo fashion (5000 simulations per sea-level rise scenario) (see Section 3.3, Table 2 and Appendix B for details). In the second step wave, wind and water level conditions of the Ems-Dollard estuary from a database developed for Dutch dike assessments (Rijkswaterstaat, 2018) were run across the accreted foreshore predicted by the deposition model in step 1 until the dike toe with the SWAN wave model (Booij et al., 1999). The Hydra-NL model (Duits and Kuijper, 2018) is

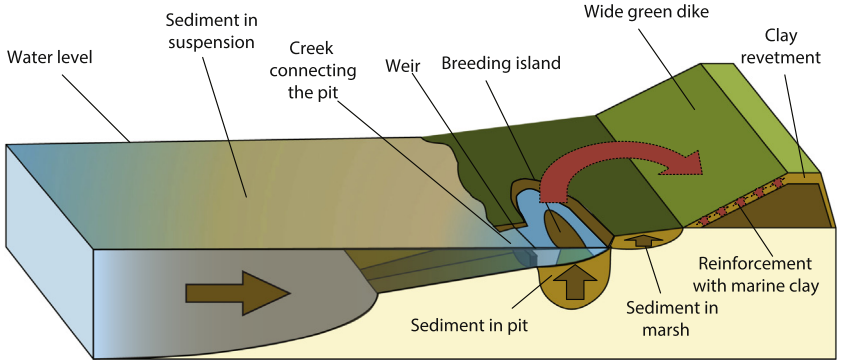

Fig. 2. A schematic cross-section of the wide green dike system and its components.

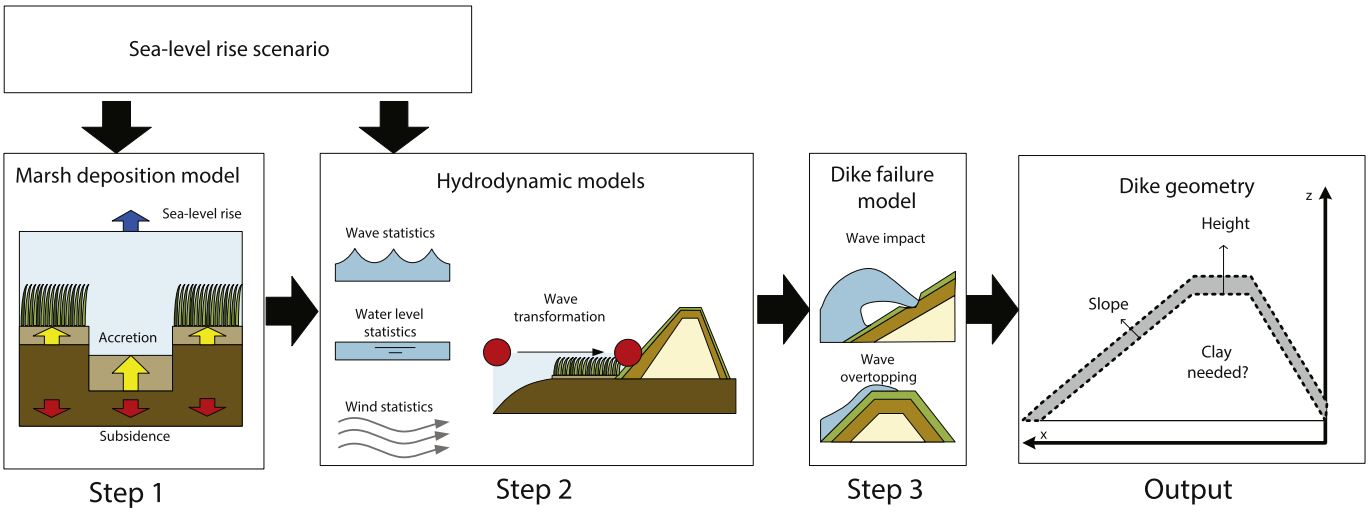

Fig. 3. The modelling approach followed in this study starting from a sea-level rise scenario towards computing the optimal dike by 2100. Step 1: determine the accumulation of sediment in the marsh, step 2: determine the storm conditions across the marsh at the dike toe, step 3: determine the probability of failure of different dike designs and return the design with the lowest clay demand as output.

used to compute the associated probability of the storm events to which correlated probability distributions were fitted. In the third step the wave and water level distributions are used to evaluate the probability of failure of different dike configurations by overtopping (van der Meer et al., 2016) and failure of the outer slope by wave action (Klein Breteler, 2015; Klerk and Jongejan, 2016; Mourik, 2015). The optimal dike configuration requires the least amount of clay to achieve the required safety level without a hard revetment. With the results of the borrow pit simulations in the first modelling step the area of pit required for 1 km of dike reinforcement is computed.

3.2. Sea-level rise scenarios

For this study the RCP and KNMI sea-level rise scenarios for the Dutch coast as presented by Haasnoot et al. (2018) were selected as a starting point (Table 1). The RCP scenarios from the IPCC were adapted by Haasnoot et al. (2018) from Le Bars et al. (2017). Dutch flood protection measures, however, were designed based on the delta scenarios that were developed in 2014 by the Royal Dutch Meteorological Institute (KNMI) (Bruggeman et al., 2013; Bruggeman et al., 2016; KNMI, 2014). The KNMI concluded that: "observations show decadal-scale variations, but no long-term trend over the past 130+ years. Results from recent state-of-the-art climate models as well as RCM studies suggest no changes in the wind climate [for the Netherlands]. This is true for mean wind conditions, low wind conditions and extreme wind speeds. Modelled changes are statistically insignificant." (KNMI, 2014, p. 69). The KNMI based this conclusion on analyses by de Winter et al. (2013) and Sterl et al. (2009). Therefore, we decided to follow the KNMI's assessment that there will be no (significant) effects of climate change on storm statistics in our study area.

The KNMI'14 scenarios do not yet account for recent findings on accelerated ice-loss (DeConto and Pollard, 2016; Haasnoot et al., 2018). No statistically significant acceleration of sea-level rise has been detected yet at stations along the Dutch coast, as the acceleration of sea-level rise accounts for just 0.1% of the variance in observed mean annual water levels (Baart et al., 2019). For this study the KNMI'14 D/R, the median of RCP 4.5, and median of RCP 8.5 scenarios were selected as a low (L), medium (M), and high (H) sea-level rise scenario for 2100. This allows for a range of possible climate change scenarios to be explored (Table 1).

3.3. Marsh deposition model

As the first step, sediment deposition within the marsh is modelled (see Fig. 3). In this study a basic marsh elevation model similar to various other studies (Allen, 1990; French, 1993; Krone, 1987; Temmerman et al., 2003) was used. It simulates a single idealised point within the marsh. Each tide when the water rises suspended sediment is transported to this point. The suspended sediment sinks towards the bottom and thus raises the elevation of this point over time. It is assumed that vegetation reduces the flow velocity such that all suspended sediment is able to sink without resuspension by turbulence. Furthermore it is assumed that the vegetation reduces wave energy and flows sufficiently to prevent settled sediment from eroding. The approach was first described by Krone (1987) and uses a mass balance as follows:

Table 1
Sea-level rise scenarios for 2050 and 2100 (in cm difference from 2018) adjusted for the Dutch coast by Haasnoot et al. (2018), using the KNMI'14 Delta scenarios and RCP scenarios. Values are adjusted by 6 cm for sea-level rise at the Dutch coast between 1995 and 2018 following Baart et al. (2019). The low (L), 50% medium (M), and 50% high (H) scenarios used in this study are highlighted in green, yellow, and red respectively.

Scenario	KNMI'14	KNMI'14		RCP			RCP	
	D/R	W/S		4.5			8.5	
Margin	-	-	5%	50%	95%	5%	50%	95%
This study	L			M			H	
2050	+ 9 cm	+ 34 cm	+ 1 cm	+ 18 cm	+ 35 cm	+ 3 cm	+ 23 cm	+ 41 cm
2100	+ 29 cm	+ 94 cm	+ 23 cm	+ 102 cm	+ 186 cm	+ 69 cm	+ 189 cm	+ 311 cm

$$\frac{dz}{dt} = \frac{dS_{min}}{dt} + \frac{dS_{org}}{dt} - \frac{dP}{dt}, \quad (1)$$

where z is the surface elevation, S_{min} the mineral sediment deposition, S_{org} is the organic deposition and P is a subsidence term. Organic deposition was omitted in this study as samples from the marsh area contained only a low percentage of organic matter (8%) indicating low organic deposition (see Appendix A).

The deposition process is described by the equations:

$$(h-z)\frac{dC}{dt} = \begin{cases} -w_s C(t) + C_{flood} * \frac{dh}{dt}\frac{dh}{dt} > 0 \\ -w_s C(t) + C(t) * \frac{dh}{dt}\frac{dh}{dt} \le 0 \end{cases} \quad (2)$$

$$\frac{dS_{min}}{dt} = \frac{w_s C(t)}{\rho_{sed}} \quad (3)$$

where h is the water level, w_s is the sediment fall velocity, C_{flood} is the suspended sediment concentration (SSC) during flood tide, $C(t)$ is the SSC at time t, and ρ_{sed} is the bulk dry density (BDD) of the deposited sediment layer.

Expanding on the approach by Temmerman et al. (2003), the expected deposition during a tidal period was modelled from the distribution of high waters and extrapolated to an annual deposition. However, to include the effect of storm surges lasting multiple cycles, the expected deposition of two tidal cycles rather than one cycle was determined in this study using a basic storm surge schematisation model for the Dutch coast (see Appendix B). We assumed no variation in SSC between storm events.

Modelling the behaviour of the borrow pit required a few additions. In order to keep water around the breeding island at low tide, a small weir was constructed in the creek draining the pit (Fig. 2). A formula was calibrated from measurements within the pit to incorporate the effect of the weir on the water level (see Appendix B). Compaction of sediment deposited within the pit was included using a variation of the formula proposed by Allen (2000a) which was calibrated with soil samples of the Dollard marsh (see Appendices A and B).

The model produces a time series of the elevation of both the marsh and the pit bed. For modelling purposes the pit is considered full when the bed elevation is within 5 cm of the marsh elevation as at this stage the difference in accretion rate between marsh and pit is no longer significant. At that point the pit is re-excavated to a depth of 1.6 m below the marsh surface identical to the pit in the pilot study. Using this setup, the amount of sediment extracted per sea-level rise scenario from that single pit is stored as a time series.

Because of uncertainty associated with multiple variables (ρ_{sed},w_s, and the initial marsh elevation z_0, see Section 4.2), a Monte Carlo approach was needed to quantify the uncertainty in accretion. The marsh deposition model was run 5000 times for each scenario, sampling randomly from the probability distributions of these variables. The median result as well as the 5 and 95 percentiles of the accretion time series were stored and passed to the next modelling steps.

3.4. Modelling storm conditions

In step 2 the design conditions for the flood defence are determined (see Fig. 3). Water-level, wave and wind statistics on the foreshore of the Dollard were retrieved from a hydraulic database of the Eastern Dutch Wadden sea (Rijkswaterstaat, 2018) and analysed in Hydra-NL (Duits and Kuijper, 2018). Hydra-NL is a programme made available by the Dutch authorities to derive hydraulic loads on flood defences across the country in compliance with the official assessments procedures (Rijkswaterstaat, 2016a). Across the Netherlands, official stations at representative locations measure water levels, wind speeds, and wind directions. Hydra-NL connects the statistical probability of the water level, wind direction, and wind speed derived from the stations, to a database of precomputed wave model simulations for the Wadden Sea area. For locations between stations values are found by interpolation. By doing so, the statistics of storm waves at the coastal defences are estimated. The correlation models employed by Hydra-NL are described in Diermanse and Geerse (2012). The effect of sea-level rise is simulated by raising the mean of the water level probability distribution accordingly (Duits and Kuijper, 2018).

A database from Rijkswaterstaat (2018) was selected which contains computed wave characteristics at the marsh foreshore in the eastern Dutch Wadden Sea under various combinations of water levels and wind conditions. This database was adapted to represent storm conditions at the dike toe per sea-level rise scenario. The widely used SWAN wave model (Booij et al., 1999) was applied across the salt-marsh profile until the dike toe for all entries in the database. SWAN uses an implicit numerical scheme to calculate the evolution of the wave spectrum across the foreshore as described by the spectral action balance equation:

$$\frac{\partial N}{\partial t} + \frac{\partial (c_{g,x} N)}{\partial x} + \frac{\partial (c_{g,y} N)}{\partial y} + \frac{\partial (c_\sigma N)}{\partial \sigma} + \frac{\partial (c_\theta N)}{\partial \theta} = S_{tot} \quad (4)$$

where N is the wave-action density, defined as spectrum energy density divided by the radian frequency, σ is the relative wave frequency. The first term describes the change in wave action over time, the second and third terms the propagation of wave action in space with velocity components $c_{g,x}$ and $c_{g,y}$, the fourth term represents the shifting of the relative frequency due to depth change, and the fifth term represents depth-induced diffraction. The sum of sink and source terms (S_{tot}) accounts for wave breaking, bottom friction, triad wave interactions, and the input of energy from the wind. The model requires an input of water level, wave spectrum properties (i.e. significant wave height, peak period, and wave direction) at the offshore boundary, an elevation profile towards the coast, and additional inputs to compute the processes included as source/sink terms (i.e. wind speed, wind direction, and bottom roughness) (Booij et al., 1999).

To simplify the computations, only a 1D profile of the marsh was used in the SWAN calculation. In this step the elevation change of the salt marsh by sedimentation (see Section 3.3) is incorporated in the foreshore profile derived from the AHN2 elevation map (Rijkswaterstaat, 2014) to examine the effect of natural sedimentation of the foreshore on the wave exposure of the dike. The effect of the pit and wave damping by vegetation was not included. A worst-case inundated tidal flat (Manning roughness) was assumed representative of winter-storm conditions. The off-shore wave boundary conditions and wind speed were retrieved from the original data of Rijkswaterstaat (2018). A new dataset of wave properties at the dike toe was created by running all entries of the original data in SWAN. The new dataset was passed to Hydra-NL to derive the statistics of wave properties at the dike. New simpler probability distributions and correlations of water level, wave height, wave period and wave direction were fitted on the outputs of Hydra-NL. For wave height and wave period a Weibull distribution was fitted, and for water level a generalized extreme value distribution was fitted. Wave direction was simplified to an empirical distribution from the wind direction, where each bin of 30° in wind direction corresponds to a generated wave direction at the dike. The result is a set of correlated probability distributions describing the frequency of storm wave- and surge conditions at the dike toe for each sea-level rise scenario which is used to design the dike.

3.5. Dike failure model

In step 3 the probability of failure for a range of dike designs is calculated (see Fig. 3). The wide green dike must be dimensioned such that the probability of failure of the dike conforms to the Dutch national safety standard (WBI2017). For this study the focus is on the main failure mechanisms that determine the outer dike geometry: overtopping and failure of the revetment by wave erosion. It was previously determined that these failures dictate the outer slope, necessitating a "wide" dike if a "green" grass revetment were to be implemented (van

Loon-Steensma and Schelfhout, 2013; van Loon-Steensma and Schelfhout, 2017). The dike section of the Dollard has a maximum annual failure probability of 1/3000. The norm for a specific cross-section failing by overtopping or erosion of the grass revetment is calculated following the Dutch design guidelines (Rijkswaterstaat, 2017) as:

$$P_{f,cross-section} = \frac{\omega}{N} P_{f,\,norm} \tag{5}$$

where the fraction of the norm failure probability ($P_{f,\,norm}$) allocated to overtopping and erosion of the revetment is 29% ($\omega = 0.29$) while the length factor (N) of these mechanisms is recommended to be 3 (Rijkswaterstaat, 2017). The result is an allowed failure probability of a cross-section ($P_{f,\,cross-section}$) of $3.22 * 10^{-5}$ year^{-1} or a minimum reliability index (β) of 4.0. Whether a dike fails by a mechanism is expressed by a limit state function (LSF). In this study the formulas accepted within the Dutch safety regulations are applied for the mechanism of overtopping and wave impact. Overtopping is a type of failure of the dike where water from waves flows over the crest onto the inner slope eroding the dike in the process. The amount of overtopping was calculated by the method described in van der Meer et al. (2016) and van der Meer (2002). The limit state has been reached when the overtopping discharge (q) exceeds the critical discharge the dike is able to resist (q_c).

$$Z_{overtopping} = q_c - q \tag{6}$$

Erosion from wave impact on the outer slope was calculated according to the descriptions in Klein Breteler (2015), Klerk and Jongejan (2016) and Mourik (2015). The limit state function is reached when the duration of the storm (t_{storm}) exceeds the amount of the time required to damage the grass (t_{grass}), the root zone (t_{root}) and erode the clay below (t_{clay}). See Appendix C for details on the calculation of each of these durations.

$$Z_{wave\ impact} = t_{grass} + t_{root} + t_{clay} - t_{storm} \tag{7}$$

The probability of failure for a dike design is determined by probabilistically evaluating the LSF's under the hydraulic boundary conditions and uncertainties with the first order reliability method (FORM) (Low and Tang Wilson, 2007):

$$\beta \underset{Z(\boldsymbol{x})=0}{=} \min\left(\sqrt{\boldsymbol{n}^T R^{-1} \boldsymbol{n}}\right) \tag{8}$$

Here β is the reliability index, $\boldsymbol{n}$ is the vector of the normalised stochastic input variables in $\boldsymbol{x}$ and R is the correlation matrix of the stochastic input variables. Vector $\boldsymbol{x}$ contains the values of the hydraulic load such as water level and wave parameters, as well as stochastic variables related to modelling wave impact and overtopping (See Appendix C). A value of variable (x_i) is normalised as:

$$n_i = \Phi^{-1}(F(x_i)) \tag{9}$$

where F is the cumulative distribution function (CDF) for that variable and $\Phi^{-1}$is the inverse standard normal CDF. The routine was programmed in MATLAB and solved for the two LSF's ($Z(\boldsymbol{x}) = 0$) with the built-in nonlinear solver called fmincon.

Since both overtopping and large wave impacts are dependent on storm conditions it is reasonable to assume both mechanisms are fully dependent. As a result, the reliability of the system is the minimum reliability of these mechanisms:

$$\beta_{system} = \min(\beta_{overtopping}, \beta_{wave\ impact}) \tag{10}$$

While the 1:7 outer slope was maintained, a range of crest height and clay thickness combinations were evaluated. The optimal outcome for each sea-level rise scenario was determined as the combination where β_{system} matched the safety standard of 4 and the required amount of clay was lowest.

4. Trust in the model system

4.1. Model selection

The series of models described in Section 3, with the exception of the marsh deposition model, were all selected for their use in and compliance with the official Dutch dike assessment instruments (WBI2017). Both the SWAN and Hydra-NL model (including their precursors) have been used extensively in determining hydraulic loads along the Dutch coast (Rijkswaterstaat, 2016a; Slomp et al., 2016). The applied overtopping and wave impact models are directly incorporated in the official Dutch dike assessment instruments or were developed specifically as an addition to these instruments (Rijkswaterstaat, 2016b). Given that these models were developed for Dutch systems already, no further validation or calibration of these models was conducted. By applying these specific models, this study will align as close as possible to the dike that would be built in practise, even if better and more advanced models are available.

Despite the fact that it is required to consider the foreshore for determining hydraulic loads on the dike (Rijkswaterstaat, 2016a), modelling the changes of the foreshore over time is not common in the Netherlands. As a result, a model had to be selected for this purpose. Highly advanced methods exist for predicting the accretion of marshes over time e.g. (Best et al., 2018; Elmilady et al., 2019; Temmerman et al., 2012), but would be computationally intensive for an exploratory study which is not focused specifically on marsh morphology. Instead a comparatively simple method employed extensively in sea-level rise studies (Allen, 1990; French, 1993; Krone, 1987; Temmerman et al., 2003) was used that could be calibrated for the Dollard estuary with the first observations from the pilot. Owing to its relative simplicity, multiple combinations of parameter inputs could be quickly assessed making this approach better suited for the study.

4.2. Implementation and evaluation of the marsh deposition model

For the implementation of the marsh deposition model suitable data of water level (h), elevation (z), sediment settling velocity (w_s), sediment density (ρ), and suspended sediment concentration in flood water (C_{flood}) is needed (see Section 3.3). For the water level (h), a record of water levels from a local gauge at Nieuwe Statenzijl was retrieved from the water authority Rijkswaterstaat and the water level within the borrow pit has been monitored as part of the ongoing pilot. The elevation of the marsh (z) was based on information from the national elevation database (Rijkswaterstaat, 2014) and checked with point measurements of the marsh taken just before implementation of the pilot (Esselink et al., 2018). Sediment characteristics on bulk dry density (ρ) were derived from local soil investigations (Raadgevend Ingenieursbureau Wiertsema & Partners, 2016; Sweco Nederland B.V., 2018) and initial measurements (Esselink et al., 2019) (see Appendix A). Sediment fall velocities (w_s) and suspended sediment concentrations (SSC) (C_{flood}) were retrieved from literature. Sediment settling velocities are reported to vary between 1 and 3 mm/s (Ridderinkhof et al., 2000; Van der Lee, 2000). There is a great variation in measured SSC in the estuary, differing between years, seasons, within spring-neap cycles and daily by weather conditions (Dankers et al., 1984; De Haas and Eisma, 1993; Dyer et al., 2000; Kornman and Deckere, 1998; Ridderinkhof et al., 2000; Taal et al., 2015; Van der Lee, 2000; van Maren et al., 2016). To generalise the model across these different seasons and conditions, a representative value for SSC during the incoming tide had to be found by calibration.

An overview of all modelling parameters is presented in Table 2. Over the period 1984–2003 the average accretion rate within the marsh has been 8 mm/yr, though large variations exist across the marsh between 0 and 20 mm/yr (Esselink, 2007; Esselink et al., 1998).

Table 2
Inputs of the model. Probability distributions: deterministic (D), empirical (E), and normal (N).

	Value	Unit	Distribution	Source
Water level				
High water peak level	From distribution	m + NAP	E	Tide gauge at Nw. Statenzijl (Rijkswaterstaat)
Sea-level rise	From scenario	m	D	See Section 3.2
Weir in borrow pit				
Weir crest elevation	0.9	m + NAP	D	(Esselink et al., 2019)
Weir flow resistance term	$R_{in} = 3.5$ $R_{out} = 2.7$ $R_{over} = 13.5$	m	D	Calibrated (see Appendix B)
Elevation				
Initial marsh elevation	$\mu = 1.86$ $\sigma = 0.12$	m + NAP	N	Based on AHN2 from Rijkswaterstaat (2014)
Initial bed elevation of the pit	0.41	m + NAP	D	Based on excavation depth of pit
Subsidence	2.6	mm/yr	D	(NCG, 2018)
Sediment				
Representative sediment concentration during flood	0.19	kg/m^3	D	Calibrated (this section)
Sediment settling velocity	$\mu = 2.7$ $\sigma = 1$	mm/s	N	(Van der Lee, 2000)
Bulk dry density of deposited sediment	$\mu = 398$ $\sigma = 87$	kg/m^3	N	See Appendix A
Bulk dry density within marsh	$\mu = 873$ $\sigma = 72$	kg/m^3	N	See Appendix A

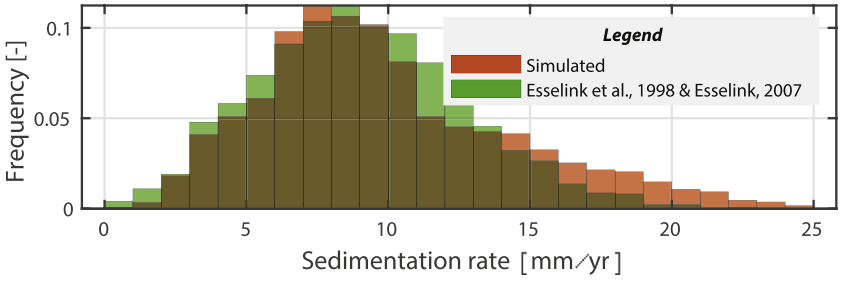

Fig. 4. Distribution of calibrated model results of the average sedimentation rate for the period 1984–2003 in orange and the distribution of measured sedimentation rates between 1984 and 2003 by Esselink in green. (For interpretation of the references to colour in this figure legend, the reader is referred to the web version of this article.)

The model was run for 1 year at elevations 0.32 ± 0.12 m above mean high tide (MHT) with different values for the representative SSC (C_{flood}). A representative SSC of 0.19 kg/m^3 best reproduced these observations (Fig. 4). To evaluate the performance of the same deposition model for the borrow pit the model was run with the exact water level time series measured at the pit between September of 2018 and March 2019, and compared the results with the deposition measured. For the initial half year of the pilot 0.13 m of elevation change was measured (Esselink et al., 2019). Subsequent measurements show a further 0.13 m of elevation change between September of 2018 and March 2019. A representative SSC of 0.25 kg/m^3 reproduced the reported elevation change (Fig. 5).

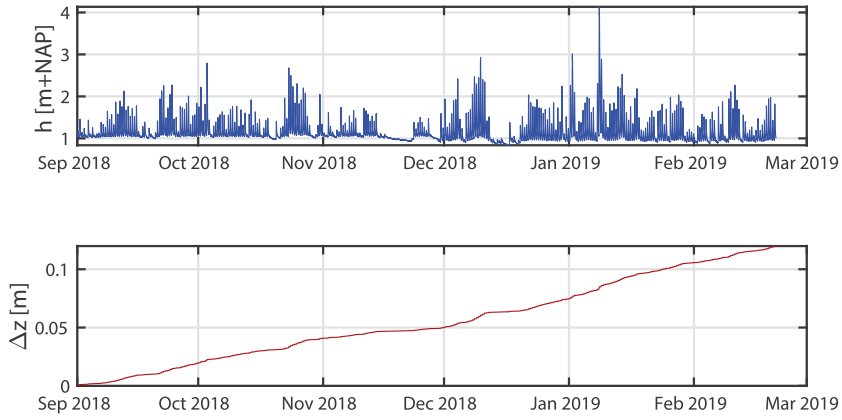

Fig. 5. Modelled sedimentation over time (bottom panel) from the water level time series measured at the borrow pit (top panel). Input parameters: $C_{flood} = 0.25$ kg/m^3; $\rho_{sed} = 372$ kg/m^3; $w_s = 2.7E{-}3$ m/s.

Both SSCs found are within the range of values that was expected from literature. A higher representative SSC of 0.25 kg/m^3 during the winter of 2018 than the 0.19 kg/m^3 for 1984 to 2003 also seems consistent with seasonal differences observed in previous studies resulting from wave action and decreased biological activity in winter (De Haas and Eisma, 1993; Dyer et al., 2000; Kornman and Deckere, 1998). For this study, however, we consider the first value of 0.19 kg/m^3 more appropriate as it was calibrated over a longer timespan with an elevation more representative for the long-term rather than the initial bed elevation of the pit. However, an extensive study of seasonal SSC variations is required to properly validate this specific value. Despite the limitations in validation we consider the model to be satisfactory for an exploratory study until validation can be performed on a longer time series.

5. Results

5.1. Marsh elevation

The predicted effect of sea-level rise on vertical accretion of the marsh surface is substantial (see Fig. 6). In the lowest sea-level rise scenario, the marsh accretes in pace with sea-level rise. For the medium scenario the deposition rate decreases until around 2050 when sea-level rise outpaces the deposition rate. From this point onward inundation depths increase with each year enhancing deposition but never catching up to the increasing rate of sea-level rise. The high sea-level rise scenario is similar to the medium scenario but is outpaced by 2035. In this scenario the marsh is projected to be below mean high water around the year 2078. Since marsh vegetation requires a minimum period of dry conditions to survive, the marsh may not persist at this stage of drowning and the assumptions underlying the model will no longer hold. That is, as vegetation cover is lost, more turbulence and wave action will inhibit sediment for settling and enable erosion. Hence, the model tends to overestimate the sediment accumulation of a drowning marsh. In a worst-case scenario, run-away erosion of the marsh could be initiated resulting in a net loss of sediment, rather than accretion.

As Fig. 6 shows, the relative water depth above the marsh during high tide does only vary in the order of centimetres between scenarios by 2050. Towards 2100 the relative water depth has remained constant for low sea-level rise, increased under medium sea-level rise and increased substantially with a high sea-level rise scenario. The 90% band of simulations decreases under strongly accelerated sea-level rise suggesting a decreasing influence of settling velocity, bulk dry density and variance in initial elevation for the deposition rate compared to the increasing inundation depth by sea-level rise. The uncertainty in initial conditions is the result of heterogenous processes in the marsh (e.g. creeks, patches of denser vegetation, etc.). The model does not capture these features, so variance across the marsh will be larger in 2100 than the model suggests. However, it does indicate that the initial uncertainty of a "representative marsh elevation" has a diminishing influence on long-term accretion trends.

5.2. Infilling of the borrow pit

For the same reasons as discussed in Section 5.1, until 2050 the expected deposition within the borrow pit is similar between scenarios until 2050 (see Figs. 7 and 8). The pit excavated in 2018 is expected to be refilled by 2040 for all scenarios. At the earliest the pit is already filled by 2029 for all scenarios in 5% of the simulations. At the latest the pit is refilled in 2068 for the low sea-level rise scenario, 2056 for the medium scenario and 2052 for the high scenario according to 95% of simulations.

The majority of infilling takes place during the initial years after excavation of the borrow pit. Within the first 10 years approximately 75% of the pit is already refilled. Initially, the relative depth to mean high tide is largest, resulting in frequent inundation and thus ample opportunities for sedimentation. Inundation frequency decreases exponentially with increasing elevation explaining the decreasing deposition within the pit over time. It further suggests that a greater initial depth of borrow pit is

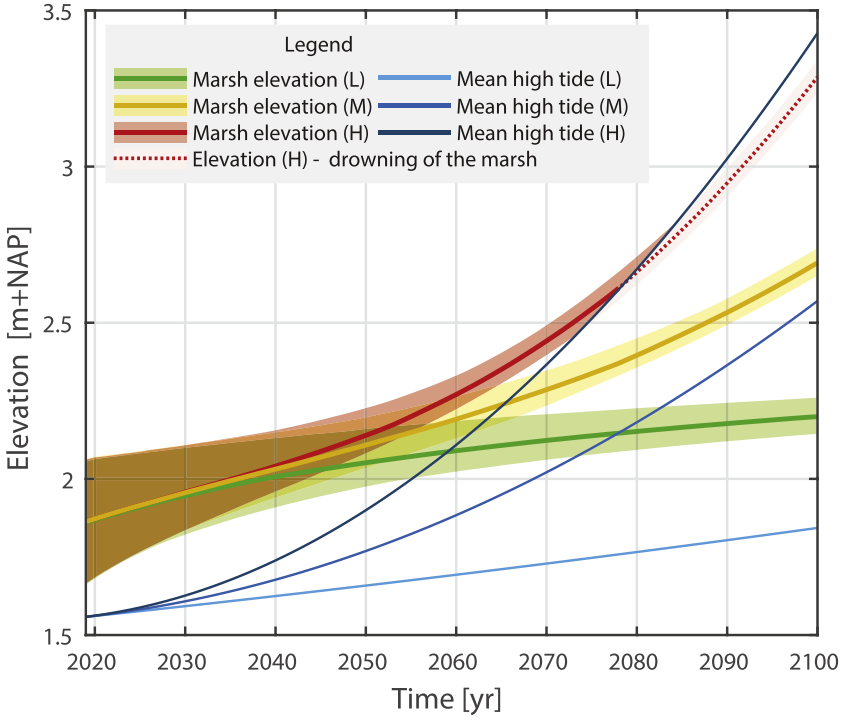

Fig. 6. Development of the marsh elevation over time as predicted by the model simulations for the low sea-level rise scenario (L) in green, medium sea-level rise scenario (M) in yellow, and high sea-level rise scenario (H) in red. The band represents 90% of simulation results and the line is the median of all simulations. (For interpretation of the references to colour in this figure legend, the reader is referred to the web version of this article.)

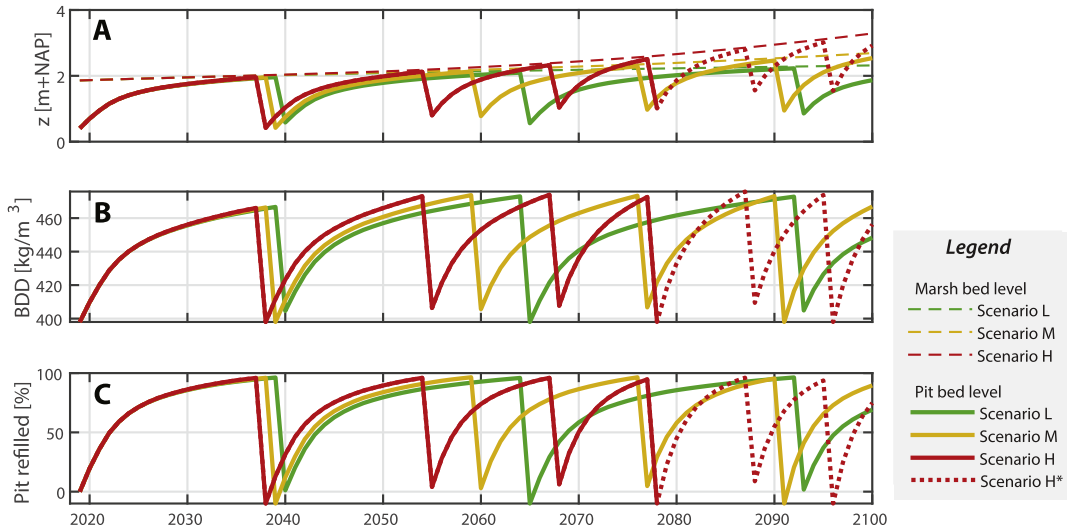

Fig. 7. The influence of sea-level rise scenario L, M and H on A) elevation, B) the bulk dry density within the pit, and C the infilling rate of the borrow pit until 2100 with all parameters fixed at average values. Note (*) that for scenario H after 2078 results are not reliable (see Fig. 6).

more efficient in capturing sediment than a pit with a shallow depth. As the rate of sea-level rise accelerates, so does the inundation frequency and thus deposition rate within the borrow pit relative to the marsh surface. The modelling results suggest an acceleration of the infilling process as a result of the acceleration in sea-level rise which results in a higher clay yield from a continuous exploitation of the borrow pit.

The model also suggests the sediment density of an infilled pit remains significantly lower than the density of the surrounding marsh, which has on average a density of 873 kg/m^3 (see Fig. 7B). On average, the infilled pit will contain only 54% of the mass of clay compared to the surrounding undisturbed marsh. The 5th and 95th percentiles of simulations show a large range in BDD within the pit upon refilling: from 37% to 74% of the BDD in the marsh. Uncertainty in the density of sediment within the pit upon re-excavation is a major influence on the total clay yield by 2100 as it directly affects the mass of clay in the pit at the end of each extraction cycle (Fig. 8).

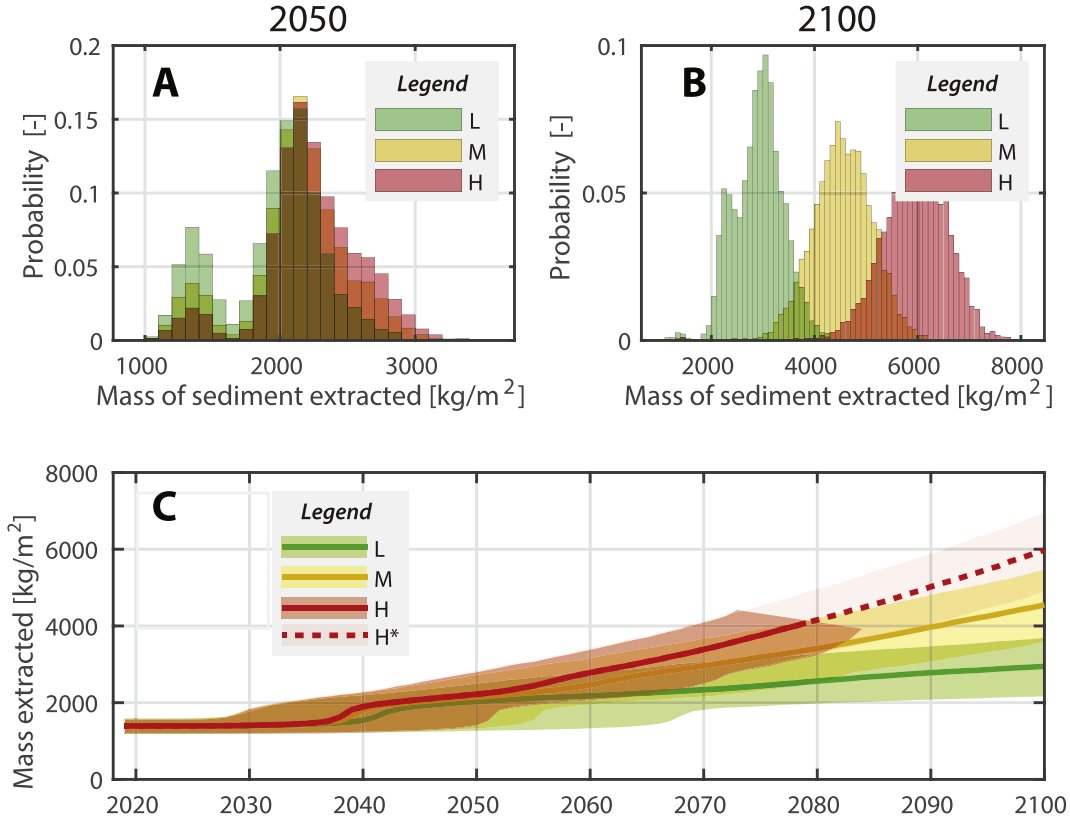

Fig. 8. The mass of clay extracted from the borrow pit by A) 2050, B) 2100 and C) cumulative over time for the low (L) sea-level rise scenario in green, the medium (M) sea-level rise scenario in yellow, and the high (H) sea-level rise scenario in red. For each scenario, the band represents 90% of all simulation results and the solid line the median. Note (*) that for scenario H after 2078 results are not reliable (see Fig. 6). (For interpretation of the references to colour in this figure legend, the reader is referred to the web version of this article.)

5.3. Optimal dike dimensions in 2050 and 2100

The deposition rate on the foreshore has a large influence on the design of the dike. If the marsh keeps pace with sea-level rise, the dike stays subjected to similar waves as initially. However, if the inundation depth increases as a result of sea-level rise the dike will be exposed to higher waves. The effects on the required dike dimensions are presented in Fig. 9. The required dike height is primarily governed by the absolute sea-level rise. Lower crest heights become increasingly likely to overtop as the water level rises. The required clay layer on the dike's outer slope is primarily affected by the impact of waves on the outer slope. For all dikes in 2050 and scenario L in 2100 the optimal thickness was found to be around 1.7 m when a 1:7 slope is maintained (Fig. 9). With increasing wave heights under extreme storm conditions, the clay layer is eroded more rapidly from wave impacts. By 2100 the required thickness has increased to 1.9 m and 2.2 in scenarios M and H respectively. In scenario H however, because of potential drowning of the marsh a lower foreshore may be present than predicted. Thus, stronger waves may reach the dike and larger dike dimensions will be required.

5.4. Matching clay demand for dikes with supply from the pits

A representative dike profile of the current Dollard dike was adapted to the dimensions calculated in Section 5.3. The amount of clay applied on the outside of the dike was computed to achieve the optimal minimal clay thickness where any space left was filled by sand. Assuming a clay density of 1200 kg/m^3 the volume of clay was converted in a demand for the mass of clay per reinforcement. This amount was converted to an area of pit using the results of Section 5.2 of the mass retrieved from each m^2 of pit (see also Supplement 2 Table S2.1).

The first reinforcement is conducted as part of the pilot in which in 2025 the dike is reinforced to the dimensions meeting the safety criteria in 2050 as calculated in Section 5.3 with clay extracted from the pit since 2018. Ordinarily dikes are reinforced for a time horizon of 50 years, but given the fact this reinforcement is part of pilot for other dike sections in the Dollard and the uncertainty in sea-level rise by 2075, a 25 years' time horizon is more applicable. The necessary area of a pit 1.6 m deep to meet the clay needed for the dike in each 2050 scenario with uncertainty margins is presented in Table 3. As the rise in sea level remains modest until 2050, there is little difference between dike dimensions and thus clay demand for each scenario. The area of pit needed lies between 4.6 and 9.4 ha with an expected area of 7.3 ha across all scenarios.

A decision will have to be made about the reinforcement strategy for 2100 based on the results of the pilot and the projected sea-level rise. We look at 2 strategies: 1) excavate a new pit elsewhere in the marsh after the first one is refilled or 2) a continuous exploitation of the same pit as shown in Fig. 8. In strategy 1 we assume 2 pits of equal of equal area are dug and refilled by 2100. In strategy 2 clay is collected until either (a) 2050 or (b) 2075. The required borrow pit area for each scenario and strategy is presented in Table 4. For a reinforcement until 2100 similarly-sized pits are needed as for a 2050 reinforcement despite the higher and thicker dikes in 2100, mostly because first the slope had to be flattened from 1:4 to 1:7. It can be seen that for the low sea-level rise scenario excavating a new pit yields more clay per hectare than excavating an existing pit once (up to 2050) or twice (2075). This is the result of the low density of clay within an infilled pit compared to the surrounding marsh. Infilling of the borrow pit is projected to accelerate with sea-level rise. As a result in scenarios M and H a large amount of additional clay can be extracted up to 2075 and cyclically excavating the pit requires less area of pit per kilometre of dike than excavating a new pit once when a reinforcement is needed.

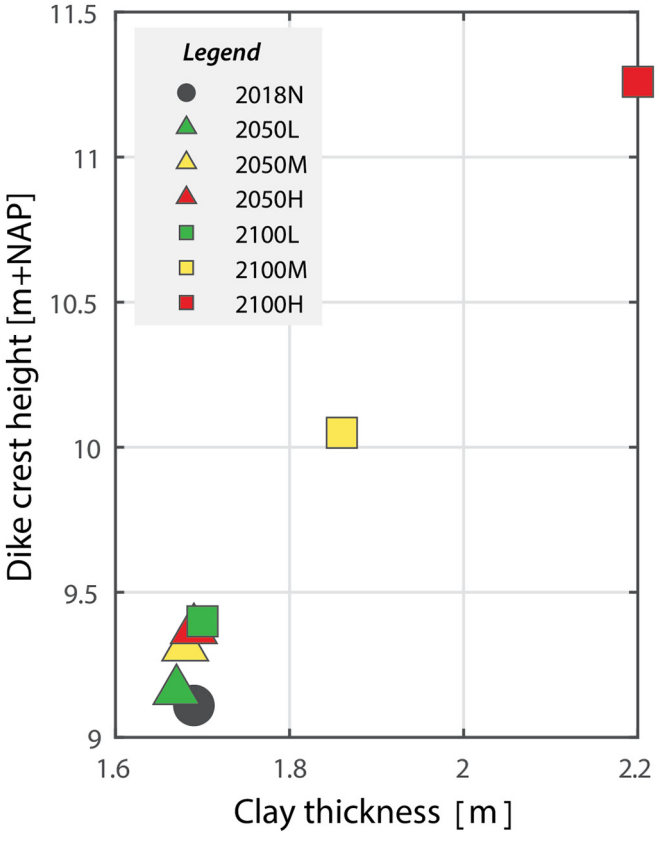

Fig. 9. The dike dimension for the three sea-level rise scenarios in 2050 and 2100 when the minimal amount of clay is applied on the dike slope. The black dot represents the optimal wide green dike design for 2018, the triangles represent 2050 dike dimensions and the squares 2100 dike dimensions. The colour of the squares and triangles indicate the sea-level rise scenario: green for scenario L, yellow for scenario M and red for scenario H. See also Table S.2.2 for the confidence bound values. (For interpretation of the references to colour in this figure legend, the reader is referred to the web version of this article.)

Table 3
The area of pit required in hectares to reinforce 1 km of dike to the 2050 safety level in the low (L), medium (M) and high (H) sea-level rise scenario with the 5%, 50% and 95% uncertainty margins.

Area of pit required (in ha) per km of dike reinforcement by 2050	L	M	H
5%	4.6	5.1	5.8
50%	7.3	7.3	7.9
95%	8.6	9.2	9.4

Table 4
The area of pit required in hectares to reinforce 1 km of dike to the 2100 safety level in the low (L), medium (M) and high (H) sea-level rise scenario with the 5%, 50% and 95% uncertainty margins.

Area of pit required (in ha) per km of dike reinforcement by 2100	L	M	H
Strategy 1: new pits			
5%	3.5	3.8	4.7
50%	4.3	4.4	5.5
95%	5.2	6.5	8.2
Strategy 2a: re-excavating pit up to 2050			
5%	4.5	4.4	5.3
50%	5.9	5.7	6.9
95%	9.9	11.7	13.8
Strategy 2b: re-excavating pit up to 2075			
5%	3.5	3.1	3.3
50%	4.9	3.8	4.1
95%	6.6	6.7	6.7

6. Discussion

Different types of nature-based solutions in flood protection have been proposed to enhance coastal protection. Ecosystems like reefs, marshes, mangroves, and oyster reefs are typically effective in wave damping and/or stabilising sediment (Narayan et al., 2016; Scheres and Schüttrumpf, 2019), but their survival and performance as flood protection measures may suffer from accelerated sea-level rise (Crosby et al., 2016; Kirwan et al., 2010; Perry et al., 2018; Ridge et al., 2015). In this regard, the ability of the ecosystems to (partially) mitigate relative sea-level rise by accumulating sediment is a more promising avenue for long-term nature-based solutions. This study explores whether utilising sedimentary processes of a salt marsh-dike system can sustainably adapt a dike system against sea-level rise. Successes of clay mining in Lower Saxony, Germany, have encouraged the concept to be reintroduced in the Netherlands (Bartholomä et al., 2013; Karle and Bartholomä, 2008; van Loon-Steensma and Schelfhout, 2017; van Loon-Steensma and Vellinga, 2019). Exploratory studies suggested a Wide Greed Dike constructed with clay from the marsh could be successfully implemented in the Dutch Dollard estuary to adapt the flood defences for future sea-level rise (van Loon-Steensma and Schelfhout, 2013; van Loon-Steensma and Schelfhout, 2017; van Loon-Steensma et al., 2014). As a result the Wide Green Dike pilot was initiated to further explore the concept (Hunze en Aa's, 2020).

Future sea-level rise has a profound effect on the implementation of an adaptation strategy involving sedimentary processes for flood protection. The first aspect relates to the vertical accretion of the foreshore. Vuik et al. (2019) demonstrated vertical accretion of the marsh contributes to flood risk reduction against sea-level rise by the dissipation of wave energy across the foreshore. A similar result was produced by the combination of a 0-D marsh deposition model and SWAN wave model in this study. When the relative water depth on the foreshore is maintained by accretion, the design storm waves will remain unchanged and only increasing the dike crest height is necessary. Otherwise reinforcement of the outer slope will be necessary.

Our simulations with the sea-level rise scenarios representing the RCP 4.5 and 8.5 scenarios of the IPCC (scenarios M and H in this study) indicate accretion rates for our case study for 2100 could be insufficient to mitigate the accelerated sea-level rise, whereas in the low KNMI'14 scenario (scenario L in this study) the marsh does keep pace with sea-level rise. Whether the marsh fronting the dike maintains its elevation relative to mean sea level until 2100 is therefore uncertain. Kirwan et al. (2010) suggested an environment like the Dollard should be capable persisting under sea-level rise upwards of 80 mm/yr but in our simulation only 9 mm/yr (90% interval: 4–12 mm/yr) could be accommodated. In the Scheldt estuary at a representative suspended sediment concentration of one fifth of the Dollard (0.04 kg/m^3) accretion was measured around 1.6 cm/yr (Temmerman et al., 2003), almost twice the accumulation rate of 8.5 mm/yr observed in the Dollard (Esselink, 2007; Esselink et al., 1998). Comparing our model parameters with the parameters from the Scheldt marsh form Temmerman et al. (2003), a high bulk dry density on the foreshore is the most important factor explaining the low deposition rate in the Dollard. Given the large influence, close consideration of bulk dry density on the foreshore is required when comparing the resilience of different estuaries to sea-level rise.

Model simulations suggest the borrow pits are expected to be refilled after 22 years (range: 11–50 years across scenarios) under present day sea-level rise rates with initial infilling in the order of 10 cm/yr and decelerating as the pit fills. This rate is comparable to the pits of Jade Bay in the German Wadden Sea, which take about 30 years to refill (Arens, 2002). Furthermore, the model predicts sediment in the refilled clay pit will not exceed a bulk dry density of 500 kg/m^3 mirroring the observations in Jade bay of former clay puts (Bartholomä et al., 2013; Karle and Bartholomä, 2008). As the infilling rate is directly related to the depth of the pit (see Section 5.2), a small yet deeper pit is more effective in trapping sediment than a wide but shallow pit. However a deeper pit will remain inundated for longer meaning it will take longer for the marsh to rejuvenate. Marsh rejuvenation was another reason for the construction of borrow pits in the Jade Bay (Bartholomä et al., 2013). In this sense the objectives of nature restoration and sediment extraction may not necessarily align.

A prediction of the model is an increasing infill rate of the pit as sea-level rise accelerates. This would be a unique property for a borrowing-pit adaptation scheme compared to other nature-based solutions in which its effectiveness increases as the sea-level rise accelerates. However, in this study it was assumed the marsh locally surrounding the pit always shelters the pit from erosion by wave action and currents. In practise the effectiveness of the borrow pit will be constrained by the adaptive capacity of the marsh to sea-level rise. Furthermore, a key assumption in this study was that the sediment concentration within the estuary would remain constant. If large scale efforts to reduce the turbidity within the estuary are successful, borrow pits being one of them, a reduced amount of sediment will be available for accumulation on the marshes and pits on the long term.

The effects of local topography and horizontal processes governing the marsh and pit were not included in the methodology for this study. However, such processes can contribute to the developments on a long timescale (Best et al., 2018; Elmilady et al., 2019). Within Jade Bay clay mining was carried out in combination with ecological restoration by redesigning an artificially developed salt marsh into a more natural marsh with natural creeks and levees (Bartholomä et al., 2013; Esselink et al., 2017). Across the pit the elevation changes varied greatly depending on emerging drainage patterns, relative elevation differences and the emergence of vegetation (Bartholomä et al., 2013; Karle and Bartholomä, 2008). Also within the Dollard marsh such differences in accretion rates exist, and which are not accounted for in our approach (Esselink et al., 1998). Such processes may hinder the capacity of the marsh to accrete locally in response to sea-level rise, resulting in e.g. the formation of ponds (Mariotti, 2016; Watson et al., 2017). Lateral erosion of the salt marsh edge also plays a role in the development of the marsh. Multiple studies have revealed collapse of the marsh can be triggered by wave action at the marsh edge, rather than by direct drowning of the marsh through sea-level rise (Fagherazzi et al., 2013; Mariotti and Fagherazzi, 2013; van de Koppel et al., 2005). This is relevant for the high sea-level rise scenarios in this study, in which an increase in wave action across the marsh was predicted. Marsh erosion from wave action leads to a smaller marsh platform, larger waves reaching the dike and thus more reinforcement of the dike. Local processes within the marsh should therefore be included in future assessments of high sea-level rise scenarios.

The use of borrow pits can be considered for other regions outside of the Dollard and the Wadden Sea as long as similar conditions can be satisfied that allow for the refilling of a pit: an abundance of suspended sediment, a sufficiently wide marsh to avoid erosive wave action at the pit, and a sufficient tidal range for sediment transport towards the marsh. Other deltas with marshes and a historic record of sediment accumulation (e.g. the Yangtze and Mississippi) should possesses these qualities unless human interventions have altered these conditions. In the Dutch case, marshes have historically been managed to further promote sediment accumulation in the marsh. Understanding the present hydrodynamics and morphology, both daily and during extreme storms, is vital to assess the balance between natural sediment accumulation, and the required sediment for flood defences. The Dutch case presented in this study allowed for the use of tools, hydrodynamic databases, and marsh monitoring efforts over decades. In the absence of such knowledge, data gathering of marsh sediment accumulation, as well as storm conditions, is necessary before the methods presented in this study can be applied.

7. Conclusions

Effective adaptation to sea-level rise is one of the major challenges of this century. The sedimentary processes within marshes fronting flood defences are an adaptation option to reinforce or improve flood defences

for future sea-level rise. Using the "Wide green dike project" in the Dutch Dollard as a case, we combined models quantifying the vertical sedimentation processes within the marsh with hydraulic models and design formulas for dike assessments to explore the feasibility of such a nature-based adaptation strategy under different sea-level rise scenarios.

For a low sea-level rise scenario (+29 cm by 2100) we simulate accretion of the foreshore in pace or faster than the rate of sea-level rise. For medium to high sea-level rise scenarios (over +102 cm by 2100) vertical accretion is outpaced by sea-level rise leading to a relatively lower foreshore and higher waves impacting the dike. As long as the marsh keeps pace with sea-level rise the grass dike can maintain an outer slope of approximately 1:7 and a clay layer of approximately 1.7 m thick. To meet safety standards by 2100 under the high sea-level rise scenario (+189 cm by 2100) the clay layer on the outer slope needs to be thickened to 2.2 m.

Clay mined from the marsh fronting the dike can supply clay for dike reinforcement. According to the model simulations the borrow pit will refill in 22 years (range: 11–50 years across scenarios) but will contain sediment of only 54% (range: 37–74%) the density of the original marsh. The model predicts that the infilling rate of the pit decreases asymptotically when the bottom elevation increases relative to the mean high tide. This results in an increasing clay yield with sea-level rise if the pits are repeatedly re-excavated upon reaching the elevation of the surrounding marsh. Depending on the scenario 7.3 ha (range: 4.6–9.4 ha) of borrow pit is necessary to reinforce the outer slope of a 1 km dike section by 2050. To construct a dike meeting the safety standards by 2100 re-excavating a new pit of 4.3 ha twice (range: 3.5–5.2 ha) is most efficient for the clay yield per hectare in the low sea-level rise scenario. In a high sea-level rise scenario with strongly accelerated sea-level rise infilling of the pit is projected to accelerate substantially. Here re-excavating a pit up to 2075 requires the smallest borrow pit of 4.1 ha (range: 3.3–6.7 ha).

This study highlights the important role sedimentary processes can play in future flood protection. Even though the study focusses on the marsh in the Dollard estuary, in principle other sediment rich estuaries suitable for marsh, e.g. within the Yangtze Delta, can utilise borrow pits in their flood protection strategies provided these pits remain sheltered from erosion within the marsh. Maintaining natural foreshores can thus be an important asset for adapting flood defences in the future.

Funding

This work is part of the Perspectief research programme All-Risk with project number P15-21, which is financed by NWO Domain Applied and Engineering Sciences.

CRediT authorship contribution statement

Richard Marijnissen: Conceptualization, Formal analysis, Methodology, Software, Validation, Visualization, Writing – original draft. **Peter Esselink:** Data curation, Investigation, Validation, Writing – review & editing. **Matthijs Kok:** Conceptualization, Funding acquisition, Project administration, Supervision, Writing – review & editing. **Carolien Kroeze:** Project administration, Supervision, Writing – review & editing. **Jantsje M. van Loon-Steensma**: Conceptualization, Funding acquisition, Project administration, Supervision, Writing – review & editing.

Declaration of competing interest

The authors declare no conflict of interest.

Acknowledgments

We would like to thank Erik Jolink from the water board Hunze en Aa's and project leader of the Wide Green Dike project for his help and collaboration that made this research possible. We would further like to thank Mark Klein Breteler from Deltares for his explanation on the assessment of clay dikes. Finally we thank Matthijs Duits at HKV for his great help in understanding and applying the Hydra-NL model.

Appendix A. Marsh soil investigations

As part of preparatory work for the pilot project of the wide green dike soil investigations have been carried out by private companies within the marsh to measure potential contamination and suitability of the clay for direct application in dike construction (Raadgevend Ingenieursbureau Wiertsema and Partners, 2016; Sweco Nederland B.V., 2018). These reports have been shared confidentially for this study. The moisture content, dry matter content, fraction of organic matter content, and the depth below the surface from which the sample were taken were recorded. Additionally the locations of the samples were recorded: at the marsh at the location of the pit, at the marsh near the clay depot (closer to the dike toe) or within one the ditches in the marsh.

Bulk dry density (BDD) of the samples was not measured and direct measurements of BDD within the Dollard marsh are limited. Esselink et al. (2019) measured BDD from 10 marsh samples. The values ranged between 744 and 1085 kg/m^3 with an average of 873 kg/m^3. Assuming the average BDD of the marsh of both Esselink et al. (2019)'s measurements and the soil investigations is the same, the properties measured in the soil investigations can be converted to BDD estimations assuming a saturation of 0.94 (see Supplement 1). This allowed for an expansion of the BDD data-set as shown by Fig. A1. BDD within the marsh varies between 737 and 1008 kg/m^3. A distinct class with higher values around 1208 kg/m^3 was found. These high values indicate clay has compacted from grazing cattle on the marsh (Esselink et al., 1998; Karle and Bartholomä, 2008).

Three measurements of BDD within the infilling borrow pit were taken by Esselink et al. (2019) measuring BDD's of 342, 367 and 407 kg/m^3. These values are comparable to the estimated BDD within ditches of the marsh. It was therefore assumed the BDD within the borrow pit will follow a similar density distribution over depth as shown in Fig. A1.

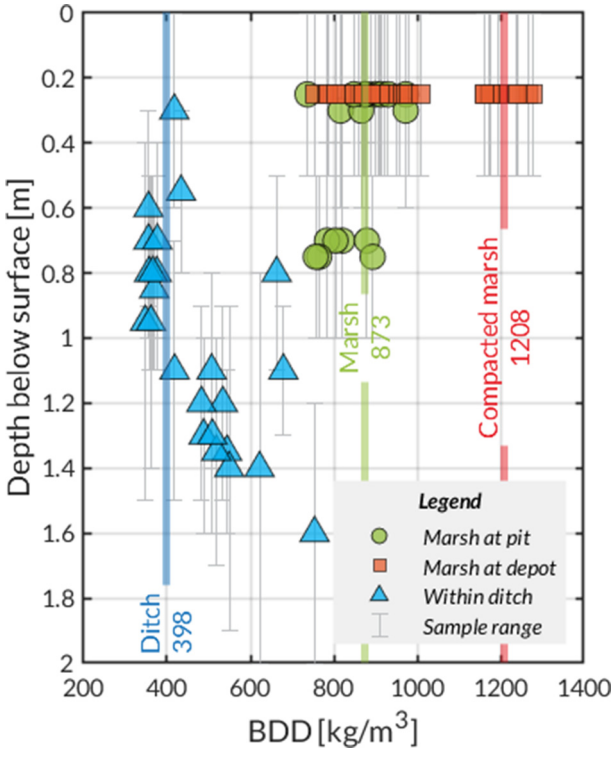

Fig. A1. Bulk dry density estimations of the marsh soil in the Dollard at three locations. The triangles were samples from a ditch, the sampled represented by circles were taken around the centre of the marsh before the borrow pit was excavated and the squares were samples close to the dike toe.

Appendix B. Simulating storm surges

B.1. The general model

The deposition within the marsh and borrowing pit is modelled using a variation of a model employed in various other studies (Allen, 1990; French, 1993; Krone, 1987; Temmerman et al., 2003). It assumes an idealised point within the marsh protected from erosion and (strong) currents by the marsh vegetation. The deposition over time () is the result of mineral deposits accumulating () organic deposits accumulating () minus subsidence of the soil () as:

$$\frac{dz}{dt} = \frac{dS_{min}}{dt} + \frac{dS_{org}}{dt} - \frac{dP}{dt}, \tag{B1}$$

Both organic deposition () and subsidence () are declared as inputs of the model. The mineral deposition part of this equation () is modelled separately. The overall sediment balance in Eq. (B1) can be resolved for large time steps. In this study Eq. (B1) was solved with an Euler forward scheme at a time step of 0.1 years with $z(0) = z_0$ as the initial condition.

The mineral deposition () occurs as a result of sediment in suspension settling on the marsh. The amount of sediment settling at a small time step depends on the concentration of suspended sediment at that time ($C(t)$) and the settling velocity of the sediment particles (w_s). The resulting elevation change from mineral deposition () is found by dividing the settled sediment mass by the sediment settling density (ρ_{sed}). This is modelled by the equation:

$$\frac{dS_{min}}{dt} = \frac{w_s C(t)}{\rho_{sed}} \tag{B2}$$

The sediment concentration ($C(t)$) is not constant over time but varies across the tide. When the water level ($h(t)$) rises, suspended sediment at a concentration (C_{flood}) is added to the water column above the marsh. When the water level decreases, suspended sediment is removed from the water column. A the same time the concentration decreases due to sediment settling. This results in equation:

$$(h(t) - z)\frac{dC}{dt} = \begin{cases} -w_s C(t) + C_{flood} * \frac{dh}{dt} & \frac{dh}{dt} > 0 \\ -w_s C(t) + C(t) * \frac{dh}{dt} & \frac{dh}{dt} \le 0 \end{cases} \tag{B3}$$

It is not feasible to run 100 years' worth of tides at the small time step required to resolve the sediment concentration part of the model. Instead, water level time series $h(t)$ lasting only two tidal cycles (T_{tide}) with a time step of 10 min were generated for many different high water events (h_{HW}) (see Appendix B.2) and used to calculate S_{min} for that event. From the local tide gauge, the probability of each high water event ($P(h_{HW})$) was determined and used to calculate the expected sedimentation:

$$E\left(\frac{dS_{min}}{dt}\right) = \frac{\sum_{i=1}^{n} S_{\min(h_i(t))} * P(h_{HW} = h_{HW_i})}{2T_{tide}} \tag{B4}$$

The expected mineral deposition was plugged into Eq. (B1) and recalculated for each time step. Given that there are about 750 high water events annually, over many years it is unlikely the actual deposition will substantially deviate from the expected deposition.

B.2. Generating water level time series during surges and within the borrowing pit

B.2.1. Storm surges

The progression of the water level during a high water event was determined the tool called "waterstandsverloop" used for Dutch dike safety assessments (HKV, 2014). The tool generates a storm surge using the tide at the location and the maximum water level during the storm as inputs. A trapezium-shaped "storm surge" is added to the tidal signal such that the maximum water level matches the highest water level of the storm. The storm duration and phase of the tide for the Dollard area were adopted directly from the report by Chbab (2015). For the case of the Dollard, the surge water level increases for 21.5 h, remains constant for 2 h before decreasing linearly over 21.5 h again. Furthermore the peak of the storm surge is taken to be 5.5 h before high tide.

To shorten the simulation time, the time series was restricted to only the two tidal cycles with the highest water levels. For the deposition model this section contains the fast rise in water level where sediment can enter the marsh and the period during high water where it settles. This extended peak of the storm is also the critical period for wave impacts at the dike as high waves are dependent on the high water level.

B.2.2. Water level within the borrow pit

The borrow pit in the Dollard is connected to the tidal network by a ditch. A weir was installed between the pit and the ditch to keep water around the bird island at the centre of the pit. This weir affects the flow of water in and out of the pit. In particular the weir prevents the pit from draining completely at low tide, allowing sediment to settle even during low tide.

Modelling the weir was achieved by incorporating the Bernoulli equation. Since the flow of the tide is orders of magnitude smaller than the flow over the weir, the flow velocity in and out of the pit over the weir is calculated as:

$$u = \sqrt{2g * \left(\hat{h} - \hat{h}_{pit}\right)} \tag{B5}$$

where and are the water depths at the sea and pit side of the weir above the level of the weir. The discharge (Q) in and out of the pit is computed as follows:

$$Q = \left(\max(h; z_{weir}) - h_{pit}\right) * R * u \tag{B6}$$

where h is the water level in the estuary, h_{pit} is the water level within the pit, z_{weir} is the elevation of the weir crest, and R is an inverse resistance term accounting for both the width of and friction induced by the weir. The change in water level within the pit is the result of discharge in and out of the pit spread out over the area of the pit:

$$\frac{dh_{pit}}{dt} = \frac{\left(\max(h; z_{weir}) - h_{pit}\right) * R * u}{A_{pit}} \tag{B7}$$

The resistance term R was calibrated for three situations: during inflow when the tide enters the pit at flood tide, during outflow when the pit drains at ebb tide, and during overflow when the tide is higher than the edges of the pit. Calibration was performed with direct measurements of the water level within the pit at the Dollard between September of 2018 and March 2019 and the local tide gauge at Nieuwe Statenzijl.

With the calibrated parameter R (Table B1) an excellent fit ($R^2 = 0.96$) was achieved between the measured water levels within the pit and the water levels converted from the tidal signal at Nieuwe Statenzijl (Fig. B1). Eq. (B7) was used to convert the water level time series generated in Appendix B.2.2 to a water level time series for the pit. The water level time series (h) in Eqs. (B3) and (B4) are substituted by h_{pit} when the accretion in the pit is being calculated.

Table B1
The parameters used to convert water levels from the tide gauge at Nieuwe Statenzijl to water levels within the pit.

Symbol	Description	Value	Unit
A_{pit}	Pit surface area	3.5	ha
z_{weir}	Weir crest elevation	0.9	m + NAP
R	Weir flow resistance term	$R_{in} = 3.5$ $R_{out} = 2.7$ $R_{over} = 13.5$	m

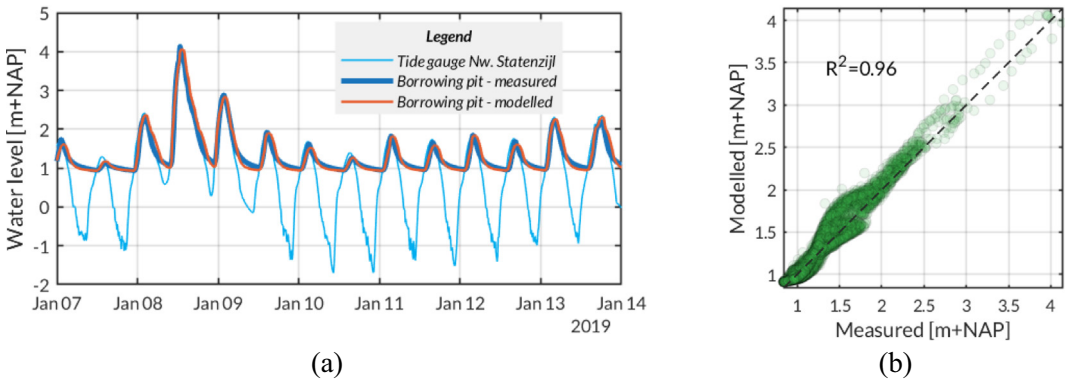

Fig. B1. (a) Comparison of the tide at Nieuwe Statenzijl (light blue) measured tide at the borrow pit (dark blue), and the modelled water level in the borrow pit over 1 week. (b) Comparison of the measured and modelled water levels in the borrow pit over a three month period. (For interpretation of the references to colour in this figure legend, the reader is referred to the web version of this article.)

B.3. Modelling auto-compaction within the pit

Allen (2000a) presented a formula to model compaction as follows:

$$T = (T_0 - T_{\min}) * e^{-kH} + T_{min} \tag{B8}$$

where T is the layer thickness, T_0 is the layer thickness during deposition, T_{min} is the minimum thickness after compaction, H is the overburden height and k is a compaction constant. For this study it is more convenient to reformulate the formula in terms of bulk dry density (ρ) and mass of sediment within the pit (m):

$$\frac{1}{\rho_{sed}} = \left(\frac{1}{\rho_0} - \frac{1}{\rho_{\inf}}\right) * e^{-km} + \frac{1}{\rho_{\inf}} \tag{B9}$$

where ρ_{sed} is the BDD of the sediment layer, ρ_0 is the BDD before compaction and ρ_{inf} the BDD after compaction. Constant k can be computed from the known profile within the ditch, the BDD of unconsolidated clay in the ditch and the consolidated clay in the marsh:

$$k = -\frac{1}{m_t} \ln\left(\frac{\frac{\rho_{inf}}{\rho_{sed}} - 1}{\frac{\rho_{\inf}}{\rho_0} - 1}\right) \tag{B10}$$

From the measurements the ρ_{inf} is taken as the BDD of the marsh and ρ_0 as the BDD at the surface of the ditch where (mostly) unconsolidated deposits are present. From the ditch measurements a BDD over depth profile was fitted:

$$\rho_{sed,ditch} = 45.53 * D^{4.284} + \rho_0 - 4.4 \tag{B11}$$

where (D) is the depth below the surface. The mass below the surface can be found by the integral:

$$m = \int \rho(D) * dD \tag{B12}$$

The deepest sample from the ditch was at 1.6 m below the surface and using expected BDD values for the marsh and ditch samples (873 kg/m^3 and 398 kg/m^3 respectively, see Appendix A), the compaction constant k can thus be estimated to be $4.6 * 10^{-4}$ kg^{-1} with uncertainty around this value. A new BDD (ρ_{sed}) accounting for compaction in the lower layers is computed for each time step of the model with the compaction constant k and the mass within the pit m using Eq. (B9).

Appendix C. Failure mechanisms

C.1. Wave impact

Failure by wave impact is considered in three stages: a) failure of the grass cover, b) failure of the roots within the clay and c) failure of the entire clay layer. In terms of a limit state approach, the failure is described by:

$$Z_{wave\ impact} = t_{grass} + t_{root} + t_{clay} - t_{wave\ impact} \tag{C1}$$

A recent study suggests adding a reduction factor for wave heights in wave impact calculations to account for lower pressures exerted by oblique waves (Klein Breteler and Mourik, 2019). However, this has not yet been implemented in Dutch dike assessment calculations and was therefore not yet considered to keep the results of this study comparable to previous designs of the wide green dike.

C.1.1. Failure of the grass cover

Within the WBI 2017 the time required for initial damage of the top layer with grass (t_{grass}) is calculated with an empirically fitted formula (Klerk and Jongejan, 2016):

$$t_{grass} = \frac{1}{C_b} \ln\left(\frac{H_s - C_c}{C_a}\right) \tag{C2}$$

where:

C_a = Constant in resistance duration curve, $[\mathrm{m}^{-1}]$

$$\text{Lognormal } (\mu = 1.82, \sigma = 0.62)$$

C_b = Constant in resistance duration curve, $\left[\mathrm{hr}^{-1}\right]$

$$\text{Constant } (-0.035)$$

C_c = Constant in resistance duration curve, [m]

$$\text{Constant } (0.25)$$

H_s = Significant wave height [m]

C.1.2. Failure of the grass and root zone

The subsequent time required to erode the clay layer reinforced by the roots of grass until 0.5 m below the surface (t_{grass}) is also determined from an empirically fitted formula (Klein Breteler, 2015):

$$t_{root} = \frac{0.5 - d_{top}}{C_d (H_s - 0.5) * (\tan\alpha)^{1.5}} \quad \text{(C3)}$$

Where:

$$C_d = Normal\left(\mu_{C_d} = 0.59 + \max(0; 8(f_{sand} - 0.7)), \sigma_{C_d} = 0.32\right)$$

d_{top} = Thickness of the top−layer of grass, [m]

(0.2 m)

H_s = Significant wave height [m]

α = Slope angle [°]

f_{sand} = Sand fraction within the clay, [%]

For clay from the pit f_{sand}<70%

C.1.3. Failure of the deeper clay layer

The time required for the remaining clay below the 0.5 m is calculated with the model by (Mourik, 2015):

$$t_{clay} = -12.66 * H_s^2 \ln\left(1 - \frac{V_e}{466 * C_e * H_s^2 * (H_s - 0.4)^2 * (\tan\alpha)^2 * \min\left(3.6; \frac{0.0061}{s_{op}^{1.5}}\right)}\right) \quad \text{(C4)}$$

V_e = the total erosion volume $[m^2]$

C_e = erosion coefficient for clay, [−]

Normal ($\mu = 0.55, \sigma = 0.1375$)

s_{op} = Wave steepness [−]

The erosion profile forming within the dike changes as erosion progresses. To greatly simplify the calculation a worst case erosion profile is assumed where the cliff side has a 1:1 (=45°) slope while the terrace is horizontal. With these assumptions the required erosion volume to erode the entire thickness of the clay layer (d) follows as:

$$V_e = \frac{1}{2} d_{clay}^2 * \left(\frac{1}{\tan\alpha} + \frac{1}{\tan(45\ ^\circ - \alpha)}\right) \quad \text{(C5)}$$

C.1.4. Wave impact duration

The zone where waves can impact the slope extends from the water line to half a wave height below the water line. The maximum duration of wave impact along any point on the slope is thus the time the water level is within a range of half a wave height of that point.

For calculations the slope is discretised in sections of wave impact zones, each with a height of 0.5 H_s. The erosion of each section is calculated using Eq. C4. When the erosion profile starts expanding into the next section, the erosion volume extending in the section above must be added to the erosion volume of the section above. From the geometry of the erosion profile the erosion volume in the next section is calculated as:

$$\Delta V_{e,i+1} = \max\left(0; 1 - \frac{1}{2} H_s * \frac{\tan(45\ ^\circ - \alpha)}{d_i}\right) * V_{e,i} \quad \text{(C6)}$$

Here d_i is the erosion depth of section i resulting in additional erosion in the next section ($\Delta V_{e,\,i+1}$). Using eq. A.4 the additional erosion is converted in additional time of wave impact exposure ($\Delta t_{wave\ impact}$) because of erosion propagating from the section below.

C.2. Overtopping

Failure of a dike by overtopping is induced by an excessive amount of waves overtopping the crest of the dike resulting in erosion of the inner slope from water flowing down the inner slope. In the limit state approach this is expressed as:

$$Z_{overtopping} = q_c - q \quad \text{(C7)}$$

Here q is the average discharge along the inner slope of the dike induced by overtopping waves while q_c is the critical discharge before erosion of the inner slope is induced. The formulas by van der Meer (2002) and van der Meer et al. (2016) are used to compute the discharge.

$$q_{\text{overtopping}} = \begin{cases} q_1 & \xi_0 < 5 \\ 10^{\frac{\log(q_1) + \log(q_2)}{2} q_2} & 5 \geq \xi_0 \geq 7 \\ & \xi_0 > 7 \end{cases} \quad \text{(C8)}$$

Of which the parameters q_1, q_2 and ξ_0 are calculated with the formulas:

$$q_1 = \min\left(\begin{array}{c} \frac{0.067}{\sqrt{\tan\alpha}} * \xi_0 * \exp\left(c_1 * \frac{z_{crest} - h}{H_s} * \frac{1}{\xi_0 * \gamma_f * \gamma_\beta}\right) \\ 0.2 * \exp\left(-2.6 * \frac{z_{crest} - h}{H_s} * \frac{1}{\gamma_f * \gamma_\beta}\right) \end{array}\right) * \sqrt{g * H_s^3} \quad \text{(C9)}$$

$$q_2 = 10^{c_2} * \exp\left(-\frac{z_{crest} - h}{\gamma_f * \gamma_\beta * H_s * (0.33 + 0.022 * \xi_0)}\right) * \sqrt{g * H_s^3} \quad \text{(C10)}$$

$$\xi_0 = \frac{\tan(\alpha)}{\sqrt{\frac{2\pi H_s}{g T_p^2}}} \quad \text{(C11)}$$

And the influence factor for the wave direction (γ_β):

$$\gamma_\beta = 1 - 0.0033 * \min(|\alpha_{wave}|, 80\ ^\circ) \quad \text{(C12)}$$

The parameters used as input are in Table C1 below.

Table C1
The input variables for the overtopping calculations.

Symbol		Description	Unit
q_c	=	Critical overtopping discharge: Lognormal($\mu = 70, \sigma = 80$)	$l^{-1}m^{-1}s^{-1}$
α	=	Angle of the outer slope	°
c_1	=	Overtopping model coefficient: Normal($\mu = -4.75, \sigma = 0.5$)	−
z_{crest}	=	Dike crest elevation	m + *NAP*
h	=	Water level	m + *NAP*
H_s	=	Significant wave height	m
γ_f	=	Slope roughness factor: 1 for grass	−
g	=	Gravitational acceleration: 9.81	$m\ s^{-2}$
c_2	=	Overtopping model coefficient: Normal($\mu = -0.92, \sigma = 0.24$)	−
T_p	=	Wave peak period	s
α_{wave}	=	Wave direction relative to the dike normal	°

Appendix D. Supplementary data

Supplementary data to this article can be found online at https://doi.org/10.1016/j.scitotenv.2020.139698.

References

Allen, J.R.L., 1990. Salt-marsh growth and stratification: a numerical model with special reference to the Severn Estuary, southwest Britain. Mar. Geol. 95 (2), 77–96. https://doi.org/10.1016/0025-3227(90)90042-I.

Allen, J.R.L., 2000a. Holocene coastal lowlands in NW Europe: autocompaction and the uncertain ground. Geol. Soc. Spec. Publ. 175 (1), 239–252. https://doi.org/10.1144/gsl.Sp.2000.175.01.18.

Allen, J.R.L., 2000b. Morphodynamics of Holocene salt marshes: a review sketch from the Atlantic and Southern North Sea coasts of Europe. Quat. Sci. Rev. 19 (12), 1155–1231. https://doi.org/10.1016/S0277-3791(99)00034-7.

Arens, S., 2002. Entwickcklung und ökologische Wertigkeit von Kleiennahmestellen in Salzwiesen - Dienstbericht Forschungsstelle Küste 14/2002. NLÖ, Norderney & Wilhelmshaven, Germany.

Baart, F., Rongen, G., Hijma, M., Kooi, H., Winter, R.d., Nicolai, R., 2019. Zeespiegelmonitor 2018; De stand van zaken rond de zeespiegelstijging langs de Nederlandse kust. Deltares, Delft, Netherlandshttps://www.deltares.nl/app/uploads/2019/03/Zeespiegelmonitor-2018-final.pdf.

Bartholomä, A., Dittmann, T., Exo, K.M., Karle, M., Metzing, D., Vöge, S., 2013. Wiederverlandung einer Pütte; Forschungsergebnisse zu Chancen un Risiken von Kleientnahmen in Salzwiesen für den Deichbauth ed. III. Oldenburgischer Deichband, Oldenurg, Germany.

Best, Ü.S.N., Van der Wegen, M., Dijkstra, J., Willemsen, P.W.J.M., Borsje, B.W., Roelvink, D.J.A., 2018. Do salt marshes survive sea level rise? Modelling wave action, morphodynamics and vegetation dynamics. Environ. Model. Softw., 109152–109166 https://doi.org/10.1016/j.envsoft.2018.08.004.

Booij, N., Ris, R.C., Holthuijsen, L.H., 1999. A third-generation wave model for coastal regions: 1. Model description and validation. J. Geophys. Res. Oceans 104 (C4), 7649–7666. https://doi.org/10.1029/98jc02622.

Borsje, B.W., van Wesenbeeck, B.K., Dekker, F., Paalvast, P., Bouma, T.J., van Katwijk, M.M., et al., 2011. How ecological engineering can serve in coastal protection. Ecol. Eng. 37 (2), 113–122. https://doi.org/10.1016/j.ecoleng.2010.11.027.

Bouma, T.J., Vries, M.B.D., Low, E., Kusters, L., Herman, P.M.J., Tánczos, I.C., et al., 2005. Flow hydrodynamics on a mudflat and in salt marsh vegetation: identifying general relationships for habitat characterisations. Hydrobiologia 540 (1), 259–274. https://doi.org/10.1007/s10750-004-7149-0.

Bruggeman, W., Dammers, E., van den Born, G.J., Rijken, B., van Bemmel, B., Bouwman, A., et al., 2013. Deltascenario's voor 2050 en 2100; Nadere uitwerking 2012–2013. Deltares, KNMI, PBL, CPB & LEI, Delft, Netherlandshttps://www.deltacommissaris.nl/binaries/deltacommissaris/documenten/publicaties/2014/05/27/deltascenarios-voor-2050-en-2100-nadere-uitwerking-2012-2013/Deltascenario%27s+voor+2050+en+2100_tcm309-351190.pdf.

Bruggeman, W., Kwadijk, J.C.J., van den Hurk, B., Beersma, J.J., van Dorland, R., van den Born, G.J., et al., 2016. Verkenning actualiteit Deltascenario's. Deltares, KNMI, PBL, Delft, Netherlandshttps://www.deltares.nl/app/uploads/2016/09/20160906-verkenning-houdbaarheid-deltascenarios-incl-bijlagen.pdf.

Chbab, H., 2015. Waterstandsverlopen Kust: Wettelijk Toetsinstrumentarium WTI-2017. Deltares, Delft, Netherlandshttp://publications.deltares.nl/1220082_002d.pdf.

Christiansen, T., Wiberg, P.L., Milligan, T.G., 2000. Flow and sediment transport on a tidal salt marsh surface. Estuar. Coast. Shelf Sci. 50 (3), 315–331. https://doi.org/10.1006/ecss.2000.0548.

Crosby, S.C., Sax, D.F., Palmer, M.E., Booth, H.S., Deegan, L.A., Bertness, M.D., et al., 2016. Salt marsh persistence is threatened by predicted sea-level rise. Estuar. Coast. Shelf S. 18, 193–199. https://doi.org/10.1016/j.ecss.2016.08.018.

Dankers, N., Binsbergen, M., Zegers, K., Laane, R., van der Loeff, M.R., 1984. Transportation of water, particulate and dissolved organic and inorganic matter between a salt marsh and the Ems-Dollard estuary, The Netherlands. Estuar. Coast. Shelf S 19 (2), 143–165. https://doi.org/10.1016/0272-7714(84)90061-1.

Davidson-Arnott, R.G.D., van Proosdij, D., Ollerhead, J., Schostak, L., 2002. Hydrodynamics and sedimentation in salt marshes: examples from a macrotidal marsh, Bay of Fundy. Geomorphology 48 (1), 209–231. https://doi.org/10.1016/S0169-555X(02)00182-4.

De Haas, H., Eisma, D., 1993. Suspended-sediment transport in the Dollard estuary. Neth. J. Sea Res. 31 (1), 37–42. https://doi.org/10.1016/0077-7579(93)90014-J.

DeConto, R.M., Pollard, D., 2016. Contribution of Antarctica to past and future sea-level rise. Nature 531 (7596), 591–597. https://doi.org/10.1038/nature17145.

DeGroodt, E.G., de Jonge, V.N., 1990. Effects of changes in turbidity and phosphate influx on the ecosystem of the Ems estuary as obtained by a computer simulation model. Hydrobiologia 195 (1), 39–47. https://doi.org/10.1007/bf00026812.

Diermanse, F.L.M., Geerse, C.P.M., 2012. Correlation models in flood risk analysis. Reliab. Eng. Syst. Safe. 105, 64–72. https://doi.org/10.1016/j.ress.2011.12.004.

Duits, M.T., Kuijper, B., 2018. Hydra-NL – Systeemdocumentatie – Versie 2.4. HKV, Lelystad, Netherlands. HKV-rapport PR3598.

Dyer, K.R., Christie, M.C., Feates, N., Fennessy, M.J., Pejrup, M., van der Lee, W., 2000. An investigation into processes influencing the morphodynamics of an intertidal mudflat, the Dollard Estuary, The Netherlands: I. Hydrodynamics and suspended sediment. Estuar. Coast. Shelf S 50 (5), 607–625. https://doi.org/10.1006/ecss.1999.0596.

Elmilady, H., van der Wegen, M., Roelvink, D., Jaffe, B.E., 2019. Intertidal area disappears under sea level rise: 250 years of morphodynamic modeling in San Pablo Bay, California. J. Geophys. Res. Earth 124 (1), 38–59. https://doi.org/10.1029/2018jf004857.

Esselink, P., 1998. Van landaanwinning naar natuurbeheer: Recente ontwikkelingen op de Dollardkwelders. In: Essink, K., Esselink, P. (Eds.), Het Eems-Dollard estuarium: interacties tussen menselijke beïnvloeding en natuurlijke dynamiek. Rijkswaterstaat Rijksinstituut voor Kust en Zee/RIKZ, Haren, Netherlands, pp. 79–99 (Rapport/RIKZ; 98.020).

Esselink, P., 2000. Nature Management of Coastal Salt Marshes: Interactions Between Anthropogenic Influences and Natural Dynamics. (Doctoral thesis). Universitry of Groningen, Netherlands (ISBN: 9036712947).

Esselink, P., 2007. Hoogteontwikkeling verwaarloosde landaanwinningskwelder: Opslibbing van de Dollardkwelders in de periode 1991–2003 en een vergelijking met de periode 1984–1991. Koeman en Bijkerk b.v., Haren, Netherlands. Report 2007-009.

Esselink, P., Dijkema, K.S., Reents, S., Hageman, G., 1998. Vertical accretion and profile changes in abandoned man-made tidal marshes in the Dollard Estuary, the Netherlands. J. Coast. Res. 14 (2), 570–582. http://www.jstor.org/stable/4298810.

Esselink, P., van Duin, W.E., Bunje, J., Cremer, J., Folmer, E.O., Frikke, J., et al., 2017. Salt marshes. In: Kloepper, S., et al. (Eds.), Wadden Sea Quality Status Report. Common Wadden Sea Secretariat, Wilhelmshaven, Germany Last updated 21.12.2017. Downloaded 01.08.2019. qsr.waddensea-worldheritage.org/reports/salt-marshes.

Esselink, P., Veenstra, W., Daniels, P., Veenstra, W., 2018. Monitoring Demonstratieproject Brede Groene Dijk (fase 1 en 2): nulmeting ontwateringsstelsel, kwelderafslag en vegetatie (2017). PUCIMAR, Vries, Netherlands (PUCCIMAR-report 16).

Esselink, P., Elschot, K., Tolman, M., Veenstra, W., 2019. Monitoring Demonstratieproject Brede Groene Dijk (fase 1 en 2): vervolgmonitoring ontwateringsstelsel, kwelderafslag, opslibbing en vegetatie (2018). PUCCIMAR, Vries, the Netherlands.

Fagherazzi, S., Mariotti, G., Wiberg, P.L., McGlathery, K.J., 2013. Marsh collapse does not require sea level rise. Oceanography 26 (3), 70–77. https://doi.org/10.5670/oceanog.2013.47.

French, J., 1993. Numerical modelling of vertical marsh growth and response to rising sea-level, Norfolk, UK. Earth Surf. Proc. Land., 1863–1881 https://doi.org/10.1002/esp.3290180105|.

Haasnoot, M., Bouwer, L., Diermanse, F., Kwadijk, J., van der Spek, A., Oude Essink, G., et al., 2018. Mogelijke gevolgen van versnelde zeespiegelstijging voor het Deltaprogramma: Een verkenning. Deltares, Delft, Netherlandshttps://www.deltacommissaris.nl/binaries/deltacommissaris/documenten/publicaties/2018/09/18/dp2019-b-rapport-deltares/DP2019+B+Rapport+Deltares.pdf.

Hallegatte, S., 2009. Strategies to adapt to an uncertain climate change. Glob. Environ. Chang. 19 (2), 240–247. https://doi.org/10.1016/j.gloenvcha.2008.12.003.

HKV, 2014. Gebruikershandleiding Waterstandsverloop. HKV, Lelystad, Netherlands.

Hunze en Aa's, 2020. Dijkversterking zeedijk - Brede Groene Dijk. https://www.hunzeenaas.nl/projecten/brede-groene-dijk/ (accessed 07-04-2020).

Karle, M., Bartholomä, A., 2008. Salt marsh sediments as natural resources for dike construction — sediment recycling in clay pits. Senck. Marit. 38 (2), 83. https://doi.org/10.1007/bf03055283.

Kirwan, M.L., Guntenspergen, G.R., D'Alpaos, A., Morris, J.T., Mudd, S.M., Temmerman, S., 2010. Limits on the adaptability of coastal marshes to rising sea level. Geophys. Res. Lett. 37 (23). https://doi.org/10.1029/2010gl045489.

Klein Breteler, M., 2015. Residual strength of grass on clay in the wave impact zone: basis for safety assessment method of WTI-2017, product 5.10. Deltares, Delft, Netherlandshttps://www.helpdeskwater.nl/publish/pages/132669/residual_strength_of_grass_on_clay_in_the_wave_impact_zone.pdf.

Klein Breteler, M., Mourik, G.C., 2019. Invloed hoek van golfaanval op graserosie op dijken. Deltares, Delft, the Netherlands (11203720-017-GEO-0001).

Klerk, W.J., Jongejan, R., 2016. Semi-probabilistic assessment of wave impact and runup on grass revetments. Deltares, Delft, Netherlandshttps://www.helpdeskwater.nl/publish/pages/132669/1220080-005-zws-0003-r-semi-probabilistic_assessment_of_wave_impact_and_runup_on_grass_revetment.pdf.

KNMI, 2014. KNMI'14: climate change scenarios for the 21st century – a Netherlands perspective. KNMI, De Bilt, The Netherlandswww.climatescenarios.nl.

van de Koppel, J., van der Wal, D., Bakker, J.P., Herman Peter, M.J., 2005. Self-organization and vegetation collapse in salt marsh ecosystems. Am. Nat. 165 (1), E1–E12. https://doi.org/10.1086/426602.

Kornman, B.A., Deckere, E.M.G.T.D., 1998. Temporal variation in sediment erodibility and suspended sediment dynamics in the Dollard estuary. Geol. Soc. Spec. Publ. 139 (1), 231. https://doi.org/10.1144/gsl.Sp.1998.139.01.19.

Krone, R.B., 1987. A method for simulating historic marsh elevations. In: Kraus, N.C. (Ed.), Coastal Sediments '87. American Society of Civil Engineers, New York, pp. 316–323.

Le Bars, D., Drijfhout, S., de Vries, H., 2017. A high-end sea level rise probabilistic projection including rapid Antarctic ice sheet mass loss. Environ. Res. Lett. 12 (4), 044013. https://doi.org/10.1088/1748-9326/aa6512.

Leonard, L.A., Croft, A.L., 2006. The effect of standing biomass on flow velocity and turbulence in *Spartina alterniflora* canopies. Estuar. Coast. Shelf S 69 (3), 325–336. https://doi.org/10.1016/j.ecss.2006.05.004.

van Loon-Steensma, J.M., 2015. Salt marshes to adapt the flood defences along the Dutch Wadden Sea coast. Mitig. Adapt. Strat. Gl. 20 (6), 929–948. https://doi.org/10.1007/s11027-015-9640-5.

van Loon-Steensma, J.M., Schelfhout, H.A., 2013. Pilotstudie Groene Dollard Dijk; een verkenning naar de haalbaarheid van een brede groene dijk met flauw talud en een breed voorland. Deltares, Alterra, Wageningen, Netherlands. Alterra-rapport 2437 (18050-000-ZKS-0004).

van Loon-Steensma, J.M., Schelfhout, H.A., 2017. Wide green dikes: a sustainable adaptation option with benefits for both nature and landscape values? Land Use Policy, 63528–63538 https://doi.org/10.1016/j.landusepol.2017.02.002.

van Loon-Steensma, J.M., Vellinga, P., 2019. How "wide green dikes" were reintroduced in The Netherlands: a case study of the uptake of an innovative measure in long-term strategic delta planning. J. Environ. Plann. Man., 1–20 https://doi.org/10.1080/09640568.2018.1557039.

van Loon-Steensma, J.M., Schelfhout, H.A., Broekmeyer, M.E.A., Paulissen, M.P.C.P., Oostenbrink, W.T., Smit, C., et al., 2014. Nadere verkenning Groene Dollard Dijk: Een civieltechnische, juridische en maatschappelijke verkenning naar de haalbaarheid van een brede groene dijk en mogelijke kleiwinning uit de kwelders. Alterra, Wageningen, Netherlands. , pp. 1566–7197. http://library.wur.nl/WebQuery/wurpubs/fulltext/302530.

van Loon-Steensma, J.M., Hu, Z., Slim, P.A., 2016. Modelled impact of vegetation heterogeneity and salt-marsh zonation on wave damping. J. Coast. Res. 32 (2), 241–252. https://doi.org/10.2112/JCOASTRES-D-15-00095.1.

Low, B.K., Tang Wilson, H., 2007. Efficient spreadsheet algorithm for first-order reliability method. J. Eng. Mech. 133 (12), 1378–1387. https://doi.org/10.1061/(asce)0733-9399(2007)133:12(1378.

van Maren, D.S., Oost, A.P., Wang, Z.B., Vos, P.C., 2016. The effect of land reclamations and sediment extraction on the suspended sediment concentration in the Ems Estuary. Mar. Geol. 376, 147–157. https://doi.org/10.1016/j.margeo.2016.03.007.

Mariotti, G., 2016. Revisiting salt marsh resilience to sea level rise: are ponds responsible for permanent land loss? J. Geophys. Res. Earth 121 (7), 1391–1407. https://doi.org/10.1002/2016jf003900.

Mariotti, G., Fagherazzi, S., 2013. Critical width of tidal flats triggers marsh collapse in the absence of sea-level rise. P. Natl. Acad. Sci. 110 (14), 5353. https://doi.org/10.1073/pnas.1219600110.

van der Meer, J.W., 2002. Technisch Rapport Golfoploop en Golfoverslag bij Dijken. TAW (TR33).

van der Meer, J.W., Allsop, N.W.H., Bruce, T., De Rouck, J., Kortenhaus, A., Pullen, T., et al., 2016. EurOtop: manual on wave overtopping of sea defences and related sturctures: an overtopping manual largely based on European research, but for worlwide application. http://www.overtopping-manual.com/.

Menke, W., 2015. Die Entwicklung des Brutvogelbestands im Elisabeth-Außengroden. In: Janssen, M., Jöns, H., Wolters, S. (Eds.), Nachrichten des Marschenrates zur Förderung der Forschung im Küstengebiet der Nordsee. Marschenrat zur Förderung der Forschung im Küstengebiet der Nordsee e. V., Wilhelmshaven, Germany, pp. 57–72.

Möller, I., Kudella, M., Rupprecht, F., Spencer, T., Paul, M., van Wesenbeeck, B.K., et al., 2014. Wave attenuation over coastal salt marshes under storm surge conditions. Nat. Geosci. 7, 727. https://doi.org/10.1038/ngeo2251.

Mourik, G.C., 2015. Prediction of the Erosion Velocity of a Slope of Clay Due to Wave Attack; Product 5.21. Deltares, Delft, Netherlands (report 1209437-017).

Narayan, S., Beck, M.W., Reguero, B.G., Losada, I.J., van Wesenbeeck, B., Pontee, N., et al., 2016. The effectiveness, costs and coastal protection benefits of natural and nature-based defences. PLoS One 11 (5), e0154735. https://doi.org/10.1371/journal.pone.0154735.

NCG, 2018. Actuele bodemdalingskaart Nederland. Nederlands Centrum voor Geodesie en Geo-Informatica (NCG)https://bodemdalingskaart.nl/ (accessed 29-11-2018).

Neumann, B., Vafeidis, A.T., Zimmermann, J., Nicholls, R.J., 2015. Future coastal population growth and exposure to sea-level rise and coastal flooding - a global assessment. PLoS One 10 (3), e0118571. https://doi.org/10.1371/journal.pone.0118571.

Nicholls, R.J., 2004. Coastal flooding and wetland loss in the 21st century: changes under the SRES climate and socio-economic scenarios. Glob. Environ. Chang. 14 (1), 69–86. https://doi.org/10.1016/j.gloenvcha.2003.10.007.

Perry, C.T., Alvarez-Filip, L., Graham, N.A.J., Mumby, P.J., Wilson, S.K., Kench, P.S., et al., 2018. Loss of coral reef growth capacity to track future increases in sea level. Nature 558 (7710), 396–400. https://doi.org/10.1038/s41586-018-0194-z.

Provincie Groningen, Ministerie van Infrastructuur en Milieu, 2018. Programma Eems-Dollard 2050. Provincie Groningen, Groningen, Netherlandshttps://eemsdollard2050.nl/wp-content/uploads/2018/03/ED2050_Rapport_DEF.pdf.

Raadgevend Ingenieursbureau Wiertsema & Partners, 2016. Onderzoek kwelderklei; Onderzoek naar de samenstelling van klei in de kwelders te Nieuwe Statenzijl en de mogelijkheden voor toepassing in een dijk, Tolbert, Netherlands. p. R40352.

Ridderinkhof, H., van der Ham, R., van der Lee, W., 2000. Temporal variations in concentration and transport of suspended sediments in a channel–flat system in the Ems-Dollard estuary. Cont. Shelf Res. 20 (12), 1479–1493. https://doi.org/10.1016/S0278-4343(00)00033-9.

Ridge, J.T., Rodriguez, A.B., Joel Fodrie, F., Lindquist, N.L., Brodeur, M.C., Coleman, S.E., et al., 2015. Maximizing oyster-reef growth supports green infrastructure with accelerating sea-level rise. Sci. Rep. UK 5, 14785. https://doi.org/10.1038/srep14785.

Rijkswaterstaat, 2014. Actueel Hoogtebestand Nederland 2 (AHN2) WMS. https://geodata.nationaalgeoregister.nl/ahn2/wms? (accessed 11-02-2019).

Rijkswaterstaat, 2016a. Regeling veiligheid primaire waterkeringen 2017: Bijlage II Voorschriften bepaling hydraulische belasting primaire waterkeringen. https://www.helpdeskwater.nl/onderwerpen/waterveiligheid/primaire/beoordelen-(wbi)/producten-wbi/.

Rijkswaterstaat, 2016b. Regeling veiligheid primaire waterkeringen 2017: Bijlage III Sterkte en veiligheid. https://www.helpdeskwater.nl/onderwerpen/waterveiligheid/primaire/beoordelen-(wbi)/producten-wbi/.

Rijkswaterstaat, 2017. Handreiking ontwerpen met overstromingskansen; Veiligheidsfactoren en belastingen bij nieuwe overstromingskans-normen. Rijkswaterstaat, Lelystad, the Netherlands https://www.helpdeskwater.nl/publish/pages/142605/handreiking_ontwerpen_met_overstromingskans_feb2017.pdf.

Rijkswaterstaat, 2018. WTI2011_Waddenzee_voorlanden.mdb. Rijkswaterstaathttps://www.helpdeskwater.nl/ (accessed 20-02-2019).

Scheres, B., Schüttrumpf, H., 2019. Enhancing the ecological value of sea dikes. Water 11 (8), 1617. https://doi.org/10.3390/w11081617.

Schuerch, M., Spencer, T., Temmerman, S., Kirwan, M.L., Wolff, C., Lincke, D., et al., 2018. Future response of global coastal wetlands to sea-level rise. Nature 561 (7722), 231–234. https://doi.org/10.1038/s41586-018-0476-5.

Slomp, R., Kolen, B., Westera, H., Verweij, J., Riedstra, D., 2016. Interpreting the impact of flood forecasts by combining policy analysis studies and flood defence. E3S Web Conf. 7, 03006. https://doi.org/10.1051/e3sconf/20160703006.

Sterl, A., van den Brink, H., de Vries, H., Haarsma, R., van Meijgaard, E., 2009. An ensemble study of extreme storm surge related water levels in the North Sea in a changing climate. Ocean Sci. 5 (3), 369–378. https://doi.org/10.5194/os-5-369-2009.

Sweco Nederland B.V, 2018. Grondstromenplan Demonstratieproject Brede Groene Dijk; Fase 1 en 2, De Bilt, Netherlands (SWNL0220816).

Taal, M.D., Schmidt, C.A., Brinkman, A.G., Stolte, W., Van Maren, D.S., 2015. Slib en primaire productie in het Eems-estuarium; Een samenvatting van vier jaar meten, modelleren, kennis bundelen en verwerven. Deltares, Imares & Rijkswaterstaat, Delfthttps://eemsdollard2050.nl/wp-content/uploads/2018/05/Slib_en_primaire_productie_in_Eems-estuarium.pdf.

Temmerman, S., Govers, G., Meire, P., Wartel, S., 2003. Modelling long-term tidal marsh growth under changing tidal conditions and suspended sediment concentrations, Scheldt estuary, Belgium. Mar. Geol. 193 (1), 151–169. https://doi.org/10.1016/S0025-3227(02)00642-4.

Temmerman, S., De Vries, M.B., Bouma, T.J., 2012. Coastal marsh die-off and reduced attenuation of coastal floods: a model analysis. Glob. Planet. Chang. 92–93, 267–274. https://doi.org/10.1016/j.gloplacha.2012.06.001.

Temmerman, S., Meire, P., Bouma, T.J., Herman, P.M.J., Ysebaert, T., De Vriend, H.J., 2013. Ecosystem-based coastal defence in the face of global change. Nature 504, 79. https://doi.org/10.1038/nature12859.

Van der Lee, W.T.B., 2000. Temporal variation of floc size and settling velocity in the Dollard estuary. Cont. Shelf Res. 20 (12), 1495–1511. https://doi.org/10.1016/S0278-4343(00)00034-0.

Vuik, V., van Vuren, S., Borsje, B.W., van Wesenbeeck, B.K., Jonkman, S.N., 2018. Assessing safety of nature-based flood defenses: dealing with extremes and uncertainties. Coast. Eng. 139, 47–64. https://doi.org/10.1016/j.coastaleng.2018.05.002.

Vuik, V., Borsje, B.W., Willemsen, P.W.J.M., Jonkman, S.N., 2019. Salt marshes for flood risk reduction: quantifying long-term effectiveness and life-cycle costs. Ocean Coast. Manag. 171, 96–110. https://doi.org/10.1016/j.ocecoaman.2019.01.010.

Watson, E.B., Wigand, C., Davey, E.W., Andrews, H.M., Bishop, J., Raposa, K.B., 2017. Wetland loss patterns and inundation-productivity relationships prognosticate widespread salt marsh loss for Southern New England. Estuar. Coast. 40 (3), 662–681. https://doi.org/10.1007/s12237-016-0069-1.

de Winter, R.C., Sterl, A., Ruessink, B.G., 2013. Wind extremes in the North Sea Basin under climate change: an ensemble study of 12 CMIP5 GCMs. J. Geophys. Res.-Atmos. 118 (4), 1601–1612. https://doi.org/10.1002/jgrd.50147.